Journal of Nanobiotechnology

RESEARCH

Open Access

Secretome enriched with small extracellular vesicles derived from human gingiva-derived mesenchymal stem cells enhances rat tongue muscle regeneration

Qunzhou Zhang[1*], Puhan He[1], Shihong Shi[1], Qilin Xu[1], Eric J. Granquist[1,2], Beth A. Winkelstein[3], Rabie M. Shanti[4] and Anh D. Le[1,2*]

Abstract

Background Accumulating evidence demonstrates that the therapeutic effects of stem cells are most likely attributed to their secretome, composed of a myriad of bioactive factors, including small extracellular vesicles (EVs). Due to the potential benefits over cells in term of handling, preservation, stability, and safety, MSC-derived secretome is emerging as a novel cell-free therapeutic for regenerative therapy of various diseases. The purpose of this study is to optimize the xeno-free culture conditions to improve the secretome production by human gingiva-derived mesenchymal stem cells (GMSCs) and test their regenerative potential using an experimental rat model of tongue muscle defect.

Methods Next-generation mRNA sequencing was performed to compare the gene expression profiles between GMSCs cultured under the defined xeno-free induction culture conditions (iGMSCs) and their 2D-cultured counterparts under regular serum-free conditions. The conditioned media (CM) from iGMSCs and 2D-GMSCs were harvested and concentrated through ultrafiltration to obtain secretomes. The EVs and soluble protein/peptide factor fractions (SPs) from the concentrated CM/secretome were separated using the 35 nm qEVoriginal size exclusion columns. The EVs were confirmed by Nanoparticle Tracking Analysis (NTA), Western blot, and transmission electron microscopy (TEM). The functional effects of secretomes derived from iGMSCs and 2D-GMSCs on macrophage polarization and skeletal muscle progenitor cells were compared both in vitro and in vivo using a rat tongue defect model.

Results Next-generation mRNA sequencing showed profound transcriptomic changes in iGMSCs compared to their 2D counterparts. Further Gene Ontology (GO)-term annotation and Gene Set Enrichment Analysis (GSEA) revealed significant upregulation of a panel of differentially expressed genes (DEGs) related to EVs and secreted cellular components (GO_CCs) and enriched pathways in oxidative phosphorylation, Wnt/β-catenin signaling, Notch signaling, and inflammatory responses in iGMSCs compared to 2D-GMSCs. iGMSC-derived CM/secretome showed a significant enrichment of both EVs and SPs compared to that derived from 2D-GMSCs, as confirmed by Nanoparticle Tracking Analysis (NTA), Western blot, and transmission electron microscopy (TEM). In vitro functional assays revealed a markedly enhanced secretion of IL-10, whilst suppressed LPS-stimulated secretion of TNF-α in macrophages treated

*Correspondence:
Qunzhou Zhang
zqunzhou@upenn.edu
Anh D. Le
Anh.Le@pennmedicine.upenn.edu
Full list of author information is available at the end of the article

with iGMSC-derived CM/secretome in comparison with that from 2D-GMSCs. In addition, iGMSC-derived CM/secretome potently induced the expression of myogenic transcriptional factors in both murine myoblasts and human skeletal muscle progenitors in comparison with 2D-GMSC-derived CM/secretome. Notably, in vivo studies using a rat tongue wound defect model, iGMSC-derived CM/secretome applied topically at the excised wound bed promoted rapid tissue repair/regeneration without fibrosis/scar and shape deformity.

Conclusion Secretome derived from GMSCs cultured under optimized xeno-free induction displayed enrichment of EVs and SPs and enhanced pro-myogenic potentials and anti-inflammatory effect on macrophages. These findings have shed light on the potential applications of the optimized iGMSC-derived secretome as cell-free therapeutics for regenerative therapy of tongue wound defects and other muscular diseases.

Keywords Gingiva-derived mesenchymal stem cells, Optimal xeno-free culture, Secretome, Extracellular vesicles, Macrophages, Skeletal muscle progenitors, Skeletal muscle regeneration, Tongue defect

Graphical Abstract

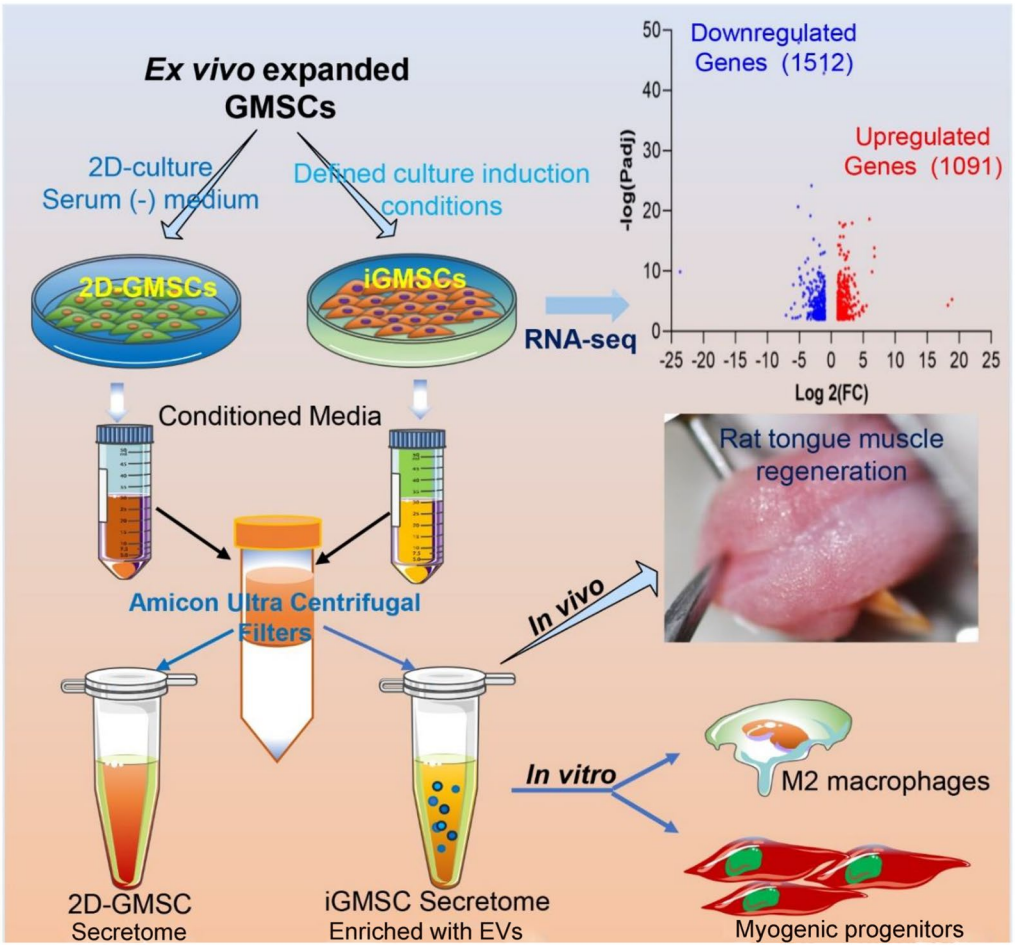

Background

Mesenchymal stem cells (MSCs) or mesenchymal stromal cells represent a unique subpopulation of postnatal stem cells that play critical roles in tissue homeostasis, regeneration and remodeling [1, 2]. In the last two decades, a similar population of MSCs has been identified and isolated from various postnatal tissues, including

but not limited to bone marrow, adipose, umbilical cord, placental and dental tissues [3–5]. In addition to their self-renewal and multipotent differentiation potentials, MSCs are recognized for their unique properties and biological functions, such as their low immunogenicity, their ability to directionally migrate to the injured/inflammatory sites, their potent immunomodulatory/anti-inflammatory functions as well as their pleiotropic antioxidant, angiogenic, and anti-senescence/apoptotic effects on other niche or neighboring cells [1, 3, 4]. These distinctive properties and functions have equipped MSCs with potent therapeutic and pro-regenerative potentials, thus highlighting their broad applicability in cell-based tissue engineering and regenerative medicine [4, 6–8]. To date, a growing body of evidence from both preclinical studies and clinical trials has demonstrated the safety and therapeutic effects of MSCs in the treatment of a large spectrum of immune and inflammatory disorders [6–8]. Traditional pharmacological drugs usually act through targeting a single pathway, but MSCs exert their therapeutic effects through multiple pathways. Rather than a simple "one stone, two birds" approach, MSCs follow a "one stone, multiple birds" model, leveraging their multipotent differentiation potentials and potent immunomodulatory/anti-inflammatory functions as well as their distinct pleiotropic effects [8–10].

It has been proposed that transplanted MSCs function through two distinct modes of action, cell replacement and paracrine bystander effects. However, a growing body of evidence has demonstrated that the major mechanism of action for MSC-based regenerative therapies involves their paracrine secretion or release of a myriad of soluble factors and extracellular vesicles or exosomes, collectively referred to as "secretome" or "conditioned media (CM)" of MSCs. This is composed of complex components such as various growth factors, cytokines, chemokines, extracellular matrix (ECM) components, DNA/RNAs, and metabolites etc. These bioactive molecules in the secretome of MSCs contribute to their immunomodulatory/anti-inflammatory functions and pleiotropic effects, and consequently, their therapeutic efficacy under various pathological conditions [3, 8, 11, 12]. Given that MSC-derived secretome or CM has been shown to replicate the multifaced functions and therapeutic efficacy of MSCs, it has emerged as a promising cell-free platform for tissue engineering and regenerative therapy of various diseases [3, 9, 10, 12, 13]. This can avoid the unfavorable adverse effects related to the use of MSCs, such as infusion-related toxicity, potential immunogenicity and tumorigenesis. In addition, MSC secretome can be lyophilized for long-term storage and convenient transportation, thus can be subjected to safety, dosage, and potency assessments similar to conventional pharmaceuticals [9, 13–15]. Accordingly, there has been an increasing number of clinical studies to evaluate the therapeutic effects of MSC-secretome/exosomes in different human disorders, including different types of wounds, osteoarthritis, diabetes, skin diseases, pulmonary diseases such as COVID-19, cardiovascular diseases, musculoskeletal diseases, neurodegenerative diseases, and oral diseases [7, 10, 13, 15, 16].

Compared to MSCs derived from other source of tissues, gingiva-derived mesenchymal stem cells (GMSCs) also possess multipotent differentiation capabilities, potent immunomodulatory/anti-inflammatory functions, and robust regenerative and therapeutic potentials in cell-based therapy of various preclinical disease models, underscoring their potential application in tissue engineering and regenerative medicine [5, 17–19]. Most recently, we have shown that local transplantation of GMSCs or their derivative exosomes significantly reduced fibrosis and promoted tongue muscle and taste bud regeneration in a tongue defect model in rats [20, 21]. In the present study, a comparative investigation was performed to assess the quality and biological functions of the secretome derived from GMSCs cultured under the optimized xeno-free induction conditions (designated as iGMSCs) as compared to the standard 2D-monolayer culture condition with serum-free medium (2D-GMSCs). mRNA sequencing revealed a significant change in the global gene expression profile, particularly an upregulation of transcripts for a panel of secreted factors and extracellular vesicles (EVs) in iGMSCs versus 2D-GMSCs. Compared to 2D-GMSCs, the conditioned medium (CM) or secretome of iGMSCs contained a significant enrichment of EVs and soluble protein factors (SPs) with enhanced dual functions on M2 macrophage polarization and myogenic transcription factor expressions in skeletal muscle progenitor cells in vitro. In vivo, iGMSC-derived CM/secretome exhibited an enhanced therapeutic effect on a tongue defect model in rats. Taken together, this study has demonstrated the establishment of optimized xeno-free induction culture conditions that significantly improved the production of GMSC-derived secretome with enhanced immunomodulatory functions and regenerative potentials, thus highlighting its potential application as cell-free therapeutics for regenerative therapy of tongue defects and some other muscular diseases.

Methods

Animals

Female Sprague–Dawley rats, weighing 200-250 g and aged from 6 to 8 weeks, were obtained from Charles River Laboratories. Rats were group-housed in polycarbonate

cages (two animals per cage) in the animal facility with a controlled temperature (23 °C ± 2 °C), 40–65% of humidity, and a 12 h light/dark cycle, fed with a standard laboratory diet and allowed ad libitum access to drinking water. All animal procedures were approved by the Institutional Animal Care and Use Committee (IACUC) of University of Pennsylvania.

Standard 2D-monolayer culture of human GMSCs

Gingival tissues were obtained as remnants of discarded tissues from healthy human subjects aged from 20–40 years old, who underwent a dental procedure following informed consents. All procedures were approved by the Institutional Review Board (IRB) at University of Pennsylvania. Primary GMSCs were routinely isolated, characterized, and maintained in our lab [18, 22, 23]. GMSCs were cultured in the complete growth medium: α-minimum essential medium (α-MEM: Invitrogen) supplemented with 10% fetal bovine serum (FBS: Zen-Bio, Inc., Durham, NC), 1% antibiotics (100U/ml penicillin/100 μg/ml streptomycin; Invitrogen), 2 mM L-glutamine, 100 mM non-essential amino acid (NEAA), and 55 μM 2-mercaptoethanol (2-ME; Sigma-Aldrich) and cultured at 37 °C in a humidified tissue-culture incubator with 5% CO_2. The adherent confluent cells were passaged with 0.05% trypsin containing 1 mM EDTA and continuously sub-cultured in the complete growth medium. Cells less than sixth passages were used in the experiments [18, 22, 23].

Establishment of optimal induction culture conditions for GMSCs to generate CM/secretome production enriched with EVs and SPs

We recently reported a nongenetic approach based on the defined culture conditions to convert GMSCs into neural crest stem-like cells with enhanced pro-nerve regeneration potentials [22]. We herein aimed to further optimize the components of the xeno-free induction culture medium for the purpose of improving the production of GMSC-derived CM/secretome with enriched EVs and bioactive SPs. In brief, tissue-treated culture (TC) dishes (100-mm) were precoated with poly-L-ornithine (PLO) at 20 μg/mL in PBS at 37 °C for 2 h. GMSCs expanded under normal culture conditions were collected and seeded onto PLO-precoated culture dishes (2×10^6 cells/dish) and cultured with the regular complete α-MEM growth medium for 24 h, whereby cells reached a confluence of 80 ~ 90%. Following extensively washed with PBS for three times, cells were cultured in 10 mL/dish of the optimized xeno-free culture medium composed of DMEM-low glucose (LG)/Ham F12 (2:1) supplemented with transferrin-depleted N2 (100×), 1% penicillin/streptomycin, non-essential amino acids (NEAA; 1×), 55 μM β-mercaptoethanol (β-ME) (all from Life Technologies), 10 ng/mL of epidermal growth factor (EGF), 10 ng/mL of basic fibroblast growth factor (bFGF) (Peprotech), and 5 μM SB431542 (Cayman Chemicals). Herein, we included EGF, bFGF, and SB431542 in the defined induction medium because EGF and bFGF are commonly supplemented in different types of defined serum-free medium to improve the proliferation and neural differentiation of MSCs [24, 25], while SB431542, a potent and selective inhibitor of the transforming growth factor-β (TGF-β) type I receptor/ALK5, has been one of the commonly used small molecules that can promote cellular reprogramming such as the generation and maintenance of iPSCs [26] and the direct reprogramming of fibroblasts into other type of cell lineages such as cardiomyocytes [27, 28]. It has also been shown that SB431542 can enhance serum-free generation of MSCs from human-induced pluripotent stem cells (iPSC-MSCs) [29] and promote the osteogenic potentials of GMSCs[30]. After culture for 3 days under this optimized culture condition (iGMSC-D3), the conditioned culture medium (CM) was harvested for secretome preparation, while cells were dissociated by trypsinization (0.05% Trypsin/EDTA), seeded into new PLO-precoated dishes (100-mm), and continued culturing for another 3 days with the optimized culture medium (iGMSC-D6). Then, the CM was harvested for secretome preparation. In parallel, cultures of GMSCs under the standard 2D-culture conditions with serum-free α-MEM medium supplemented with 1% penicillin/streptomycin served as controls (2D-GMSCs).

Culture of skeletal muscle progenitor cells and Raw264.7 macrophages

C2C12, an immortalized murine myoblast cell line obtained from ATCC (CRL-1772™), was maintained and sub-cultured in growth medium, Dulbecco's Modified Eagle's Medium (DMEM) with high glucose (HG) supplemented with 10% FBS and 1% antibiotics. Human Skeletal Muscle Satellite/Stem Cells (hSkMuSC) obtained from ScienCell Research Laboratories (Cat. No. 3510) were maintained and sub-cultured with Skeletal Muscle Cell Medium (SkMCM, Cat. #3501) according to the manufacturer's protocol (ScienCell Research Laboratories). RAW 264.7, a murine macrophage cell line obtained from ATCC (TIB-71™), was maintained and sub-cultured in DMEM-HG supplemented with 10% FBS and 1% antibiotics. All cells were cultured at 37 °C in a humidified tissue-culture incubator with 5% CO_2.

RNA extraction, library construction, and RNA-seq

RNA was extracted from GMSCs cultured under standard 2D-culture conditions with 2% exosome-depleted FBS or optimized xeno-free culture conditions using the

TRIzol reagent (Invitrogen, Carlsbad, CA). RNA concentration and purity was measured using a NanoDrop 2000 Spectrophotometer. The extracted RNAs were analyzed on BioAnalyzer nano chip to check for quality. The RINs (RNA Integration Number) were 7.5 or above. The mRNA-Seq libraries were made using Illumina Stranded mRNA library kit. After checking for quality and quantitation on a BioAnalyzer the libraries were pooled equimolarly. The pool was initially sequenced on a MiSeq nano flowcell to check for pool balance and percent reads aligning to transcriptome. The pool was adjusted by adding more volumes of the low-performing libraries. This was followed by a production run on 1 lane of NovaSeq 6000 using S1 flowcell and 100 bp SR sequencing, 300 pM pool and 1% phiX. The number of reads obtained was between 51 and 106 M. Sequence data in BCL format was converted to FASTQ and demultiplexed using bcl2fastq2. Reads were not trimmed but were interrogated for adapter statistics. MD5 checksums were generated for, and Fastqc was run on FASTQ files. Data was distributed via PSOM HPC cluster and PennBox (Penn Genomic & Sequencing Core at Perelman School of Medicine, University of Pennsylvania).

Bioinformatic analysis for RNA-seq data

On the PennHPC, Salmon was used to count the trimmed data against the transcriptome optimized in Gencode v43, which was built on the genome GRCh38. QC analyses were done with Fastqc for the raw fastq files. On a local workstation, several Bioconductor packages in R were used for subsequent analyses. The transcriptome count data was annotated and summarized to the gene level with tximeta and further annotated with biomaRt. PCA analysis and plots were generated with PCA tools. Normalizations and statistical analyses were done with DESeq2. Clustering, QC, gene expression, and volcano plots were performed with the DEGreport package. Differentially expressed genes (DEGs) were optimized as genes with log2 fold-change (FC) > 1 between conditions and adjusted P value < 0.01. Heatmap of globe differentially expressed genes (DEGs) were also visualized by the same online tool. Advanced pathway analyses was done by Gene Set Enrichment Analysis (GSEA) in pre-ranked mode with the DESeq2 statistic value as the ranking metric, whereby differentially expressed genes of each cluster were pre-ranked by differential test-statistic and analyzed using the H: Hallmarks and C2: canonical pathways geneset collections [31]. Functional annotations and functional gene enrichment analysis of the DEGs identified in GMSCs under optimized induction culture conditions (iGMSCs) versus the control 2D-GMSCs were performed using the online DAVID database (2021 update) [32], which incorporates Gene Ontology (GO) Terms, KEGG (Kyoto Encyclopedia of Genes and Genomes) pathways, and UniProtKB Keywords (UP_KW) protein domains and interactions. GO depicts three main biological concepts: biological process (BP), molecular function (MF) and cellular component (CC). The enriched annotation terms with p value ≤ 0.05 was selected and shown according to the online results[32].

Preparation of the concentrated conditioned medium (CM) or secretome derived from 2D-GMSCs and iGMSCs

The same volume of fresh conditioned culture medium (CM) derived from a similar number of 2D-GMSCs, iGMSC-D3, and iGMSC-D6 (10 mL/2 × 10^6 cells) was harvested and immediately centrifuged at 1000 × g for 20 mina at 4 °C to remove cells and large debris. The supernatant was filtered through syringe filters with a 0.22 µm hydrophilic PVDF membrane (Thermos Fisher Scientific). The pre-processed CM was further concentrated about 100 times (e.g. from 10 mL to 0.1 mL) through ultrafiltration using the Ultracel®-10 KDa Amicon® Ultra-15 Centrifugal Filters (Merk Millipore Inc.), and washed twice with 10 mL of PBS before obtaining the final concentrated CM/secretome products so as to minimize the remnant of supplements (e.g. EGF, bFGF, and SB431542) in the defined xeno-free medium [33]. The protein concentration of secretomes was measured using the Pierce™ BCA Protein Assay kit (Thermo Scientific) following the manufacturer's instructions. The concentrated CM/secretome was either used for separation of EVs and EV-free SPs or stored in aliquots at − 80 °C for further use with limited freeze–thaw cycles to avoid the negative effect on the bioactivity.

Functional assays of the CM/secretome derived from iGMSCs and 2D-GMSCs

Immunomodulatory effects on macrophages

Raw 264.7 macrophages were seeded into 12-well culture plates (1 × 10^5/well). After overnight culture, the media were replaced with 2 mL of fresh complete culture medium supplemented with 2.5 µl, 5 µl, and 10 µl of 100 × concentrated CM/secretome, equivalent to 250 µl (12.5%), 500 µl (25%), and 1000 µl (50%) of the original CM, respectively [34, 35]. Following culture for 48 h, the supernatants were collected for ELISA assay on the secretion of IL-10. On the other hand, Raw264.7 macrophages seeded in 12-well culture plates (1 × 10^5/well) were pretreated with 2.5 µl, 5 µl, and 10 µl of 100 × concentrated CM/secretome supplemented in 2 mL complete culture medium for 2 h, followed by culturing in the presence or absence of 100 ng/mL lipopolysaccharide (LPS; Sigma) for 24 h. The supernatants were then collected for ELISA assay on the secretion of TNF-α.

Pro-myogenic potential assay

Murine C2C12 myoblasts or hSkMuSCs were seeded into 6-well culture plates (2×10^5/well) with the growth medium. After overnight culture, the media were replaced with 2 mL of fresh growth medium supplemented with 2.5 µl, 5 µl, and 10 µl of 100×concentrated CM/secretome and cells were cultured for 48 h. Afterwards, cells were harvested and the whole cell lysates were prepared for Western blot analysis on the protein expression of myogenic transcription factors.

Enzyme-linked immunosorbent assay (ELISA)

Following treatment with different concentrations of the concentrated CM/secretome of GMSCs or iGMSCs, the secretion level of IL-10 or TNF-α in the supernatants of Raw264.7 cells or LPS-stimulated Raw264.7 cells was detected using the ELISA MAX™ Deluxe Sets according to the manufacturer's protocols (BioLegend; San Diego, CA), respectively.

Separation of extracellular vesicles (EVs) and soluble protein factors (SPs) through size-exclusion chromatography (SEC) and ultrafiltration

The 35 nm qEVoriginal size exclusion columns (Izon 35) were used to separate the EVs and SP fractions from the concentrated CM/secretome according to the manufacturer's manuals as described previously [33, 34, 36]. Briefly, the qEV35 columns were pre-washed and equilibrated with PBS followed by loading 500 µl of concentrated CM/secretome samples on top. Afterwards, the column was topped up with 3 mL filter-sterilized 1×PBS and eluted with each fraction of 0.5 mL collected. In total, the column was eluted with 15 mL PBS. The concentration of EV nanoparticle and protein content in each fraction was determined using ZetaView instrument and BCA analysis, respectively. Accordingly, EV-enriched fractions 5–8 and EV-free SP fractions 17–26 enriched with protein/peptides were pooled, respectively. The pooled eluent fractions were subjected to ultrafiltration using the Ultracel®-10 KDa Amicon® Ultra-15 Centrifugal Filters (Merk Millipore Inc) and concentrated to the original volume (e. g. 500 µl) of the concentrated CM/secretome sample loaded onto the qEV column. The protein concentration of separated EVs and SPs was measured using the Pierce™ BCA Protein Assay kit (Thermo Scientific) following the manufacturer's instructions. All EV and EV-free SP samples were stored in aliquots at − 80 °C for further characterization and use.

Nanoparticle tracking analysis (NTA) with ZetaView

All isolated EV samples were measured with ZetaView PMX 110 Instrument (Particle Metrix, Meerbusch, Germany) [37]. Briefly, EV samples were diluted in 1×PBS to a final volume of 1 mL and the ideal measurement concentrations were determined by pre-testing the ideal particle per frame value with the manufacturer's default software settings for EVs or nanospheres. The diluted samples were loaded into the ZetaView Cell for particle analysis to obtain the diameter size (mode), size distribution, and the particle concentration at a controlled temperature of 23 °C. Three cycles were performed for each sample by scanning 11 different cell positions and capturing 30 frames per position under appropriate settings. After capture, the videos were analyzed by the in-built ZetaView Software 8.04.02 SP2 with specific analysis parameters [37]. All the measurements were performed by the Extracellular Vesicle Core at University of Pennsylvania School of Veterinary Medicine (https://www.vet.upenn.edu/research/core-resources-facilities/extracellular-vesicle-core/evc-services).

Transmission electron microscopy (TEM)

The structure of isolated EVs was assessed by Transmission electron microscopy (TEM). Briefly, 10 µl of each sample was adsorbed to an ultra-thin carbon-coated 400 mesh copper grid and fixed in 2% glutaraldehyde. Then, the grids were negatively stained in two consecutive drops of 1% uranyl acetate with methylcellulose to increase the contrast of the membrane structure, while the excessive stain was quickly blotted and aspirated. The grids were visualized using a TEM with an FEI T12 transmission electron microscope. All the assessments were performed by the Electron Microscopy Resource Lab of University of Pennsylvania Perelman School of Medicine (https://www.med.upenn.edu/electronmicroscopyresourcelab/negative-stain-em-instrumentation).

Western blotting analysis

To assess the enrichment of EV protein markers or soluble protein factors in concentrated CM/secretomes or purified EV samples, equal amount of each concentrated CM/secretome or EV sample (15 µl) was mixed with Laemmli loading buffer and boiled at 95 °C for 5 min. For whole cell lysates from cultured cells, total protein was extracted using RIPA lysis buffer and equal amount of each protein sample (30 µg) was mixed with loading buffer and boiled at 95 °C for 5 min. The denatured samples were separated on 12% sodium dodecyl sulfate (SDS)-polyacrylamide gel and electroblotted onto Amersham™ Protran™ Nitrocellulose Blotting Membrane (Cat#10,600,002; Cytiva). After blocking with 5% nonfat dry milk in 1×Tris-buffered saline containing 0.1% Tween-20 (TBST), the membrane was incubated with appropriate primary antibodies at 4 °C overnight. Following incubation with a corresponding horseradish peroxidase (HRP)-conjugated secondary

antibodies at room temperature for 1 h, blot signals were developed with ECL™ Western Blotting Detect Reagents (GE Health Care) and images were captured using Amersham Imager 680 (GE Health Care Life Sciences). Afterwards, the membranes were stripped with Restore™ Western Blot Stripping Buffer (Thermo Scientific; 21,059) and the blots were re-probed with a specific antibody against β-actin as an internal loading control [21, 22]. All the primary and secondary antibodies used were listed in Additional file 1: Table S1.

Animal Surgery

Rat tongue defects were created according to our previous studies[20, 21]. Following anesthesia via intraperitoneal administration of ketamine/xylazine (100/10 mg/kg) and local application of 1% lidocaine into the left hemitongue, a tongue wound was created using a 6-mm biopsy punch (Miltex, Inc., York, PA, USA) in the left side of anterior dorsal tongue surface at the depth (3 mm) of the muscle layers to excise both the epithelium and the stroma. Animals were randomly divided into the following groups (n = 6/group): 1) Tongue defects patched with a strip of decellularized porcine small intestinal submucosa extracellular matrix membrane (SIS-ECM 2.0; Cook Biotech, Inc., West Lafayette, IN); 2) Tongue wound defects treated with local application of 30 µl of Tisseel, a commercially available fibrin sealant (Baxter) and patched with a strip of SIS-membrane (SIS/Fibrin); 3) Tongue wound defects treated with local application of 30 µl of Tisseel mixed with the concentrated 2D-GMSC-CM/secretome and patched with a strip of SIS-membrane (SIS/Fibrin/GMSC_CM); 4) Tongue wound defects treated with local application of 30 µl of Tisseel mixed with the concentrated iGMSC-CM/secretome and patched with a strip of SIS-membrane (SIS/Fibrin/iGMSC_CM). Based on the protein concentration of the concentrated CM/secretome, an equal amount of 50 µg of CM/secretome (in term of the protein content including both EVs and SPs) derived from 2D-GMSCs and iGMSC-D6 was locally applied with Tisseel. The SIS membranes were patched over the wound 8–0 Ethilon (Ethicon, Inc., Somerville, NJ, USA) interrupted sutures were applied to secure the membrane. The entire procedure was performed under a surgical microscope (Global Surgical Corporation, St. Louis, MO, USA). 6 weeks post-surgery, the tongue of rats from each group was photographed using a Nikon D90 digital camera with an AF Micro NIKKOR 60 mm lens. Then, rats were sacrificed and the tongues were harvested by transection at the circumvallate papillae and subsequently prepared for histological and immunohistochemical analysis.

Histological and immunofluorescence studies

The rat tongue samples were fixed in 10% neutralized formalin for 48 h and 5 µm-thick paraffin sections and 10 µm-thick cryosections were cut, respectively. Hematoxylin and eosin (H & E) staining was performed according to the standard procedures using paraffin sections, while immunofluorescence studies were conducted using cryosections. After permeabilization in 0.5%Triton X-100 for 20 min and blocking with 2.5% goat serum in PBS at room temperature for 1 h, the cryosections were incubated with primary antibodies overnight at 4 °C. The primary antibodies include desmin (1:400; ProteinTech), CD68 (1:200; Bio-Rad), arginase-1 (1:400; ProteinTech), iNOS (1:400; ProteinTech). Following washing, the sections were incubated with appropriate fluorescein-conjugated secondary antibodies at room temperature for 1 h, including Alexa Fluor®-488 Donkey anti-rabbit IgG (minimal x-reactivity) antibody (406,416; 1:300, BioLegend) and Alexa Fluor®-588 goat anti-mouse IgG (minimal x-reactivity) antibody (405,326; 1:300, BioLegend). Isotype-matched control antibodies (BioLegend, San Diego, CA) were used as negative controls. Nuclei were counterstained with 4', 6'-diamidino-2-phenylindole (DAPI) (Life Technologies, Carlsbad, CA). Images were observed and captured with a fluorescence microscope (Olympus IX-73) [23]. To quantify the expression of arginase-1 or iNOS (in red color) within $CD68^+$ (in green color) macrophages, the area of colocalized immunolabeling signals (in yellow-orange pixels) in the merged files was measured using ImageJ program and presented as the percentage of colocalization = the area of yellow-orange pixels/total area of green pixels[38].

Statistical analysis

All data were expressed as mean ± standard error of measurement (SEM) and all statistical analyses were carried out using GraphPad Prism 10.0 (IBM, Inc., Armonk, NY, USA). Direct comparisons between experimental and control groups were analyzed by paired Student's *t-test*. One-way analysis of variance (ANOVA) was employed for multiple comparisons. Post-hoc pairwise comparison between individual groups was performed using Tukey's test. A *P*-value of less than 0.05 was considered statistically significant.

Results

Establishment of optimized xeno-free induction culture of GMSCs

Previously isolated, characterized, and cryopreserved GMSCs were propagated and ex vivo expanded under 2D monolayer culture conditions [18, 22, 23]. The ex vivo expanded GMSCs were seeded into regular non-coated

100-mm TC culture dishes or PLO-precoated 100-mm TC culture dishes (2×10^6 cells/dish) and cultured with regular complete α-MEM growth medium for 24 h, whereby cells reached a confluence of 80 ~ 90% (Additional file 2: Figure S1a, b). Afterwards, GMSCs in non-coated dishes were switched to culture with 10 mL/dish of serum-free α-MEM medium (designated as control 2D-GMSCs), while cells in PLO-precoated dishes were switched to culture with 10 mL/dish of the defined or optimized xeno-free induction medium (designated as iGMSCs) as described in Materials & Methods (Additional file 2: Figure S1a).

After 72 h, cells cultured under the serum-free 2D-culture condition maintained the spindle shape (2D-GMSCs)) (Additional file 2: Figure S1b, the right upper panel), while those cultured in PLO-precoated TC dishes with the optimized induction medium exhibited a more aligned pattern (iGMSCs) (Additional file 2: Figure S1b, the right lower panel). After harvesting the conditioned medium, iGMSCs were dissociated by trypsinization and seeded back to new PLO-precoated TC dishes and continued culturing with the optimized xeno-free induction medium for another 72 h (Additional file 2: Figure S1a). 24 h later (day 4), the cells underwent remarkable morphological changes characterized by a relative homogeneity with a round shape and smaller cell size (Additional file 2: Figure S1c, the left panel). 72 h later, some of the cells aggregated to form 3D-spheroid-like structures (Additional file 2: Figure S1c, the right panel). These results suggest that GMSCs cultured under the optimized induction conditions (iGMSCs) underwent remarkable phenotypic changes compared to 2D-GMSCs.

Changes in the global gene expression profiles in iGMSCs compared to 2D-GMSCs

We then performed next-generation sequencing of mRNA to examine the changes in the global gene expression profiles between 2D-GMSCs and their counterparts cultured under the optimized induction conditions for 72 h (designated as iGMSC-D3), and those for another round of 72 h (designated as iGMSC-D6) from five different donors, that is, five libraries for 2D-GMSCs, five for iGMSC-D3, and five for iGMSC-D6, respectively (Additional file 2: Figure S2a, Fig. 1a). Compared to 2D-GMSCs, cells cultured under the optimized induction condition for 72 h has already underwent significant changes in the transcriptome, whereby the significant transcriptome differences between 2D-GMSCs and iGMSC-D3 was presented by the heatmap of differentially expressed genes (DEGs) (Additional file 2: Figure S2a). Meanwhile, the Volcano plots show a total of 773 DEGs (Cutoffs: abs (Ifc) > 1.0 and FDR or *padj* value < 0.01) with 380 upregulated and 393 downregulated (Additional file 2: Figure S2b). The top 50 DEGs that are upregulated or downregulated in iGMSC-D3 versus 2D-GMSCs are listed in Additional file 3: Table S2 and Additional file 4: Table S3, respectively. Notably, more pronounced transcriptome alterations were observed in GMSCs following culturing under the optimized induction condition for another round of 72 h (iGMSC-D6) compared to 2D-GMSCs as presented by the heatmap and Volcano plots of DEGs (Cuttoffs: abs (Ifc) > 1.0 and FDR or *padj* value < 0.01), wherein a total of 2603 DEGs were identified with 1091 upregulated and 1512 downregulated (Fig. 1a, b). The top 100 DEGs that are upregulated or downregulated in iGMSC-D6 versus 2D-GMSCs are listed in Additional file 5: Table S4 and Additional file 6: Table S5, respectively.

Pathway enrichment and functional gene annotation analyses

Next, we performed gene functional annotation and pathway enrichment analyses of DEGs identified in iGMSC-D3 which were cultured under the optimized induction condition for 72 h. Gene Set Enrichment Analysis (GSEA) revealed several enriched pathways in iGMSC-D3 *versus* 2D-GMSCs, including oxidative phosphorylation (NES: 2.18343; FDR q-value: 0.0), fatty acid metabolism (NES: 1.842387; FDR q-value: 0.0), glycolysis (NES: 1.723982; FDR q-value: 0.0), PI3K/Akt/mTOR signaling pathway (NES: 1.5176543; FDR q-value: 0.011993174), and protein secretion (NES: 1.8853154; FDR q-value: 0.0) (Additional file 2: Figure S2c-g). Using DAVID Gene Functional Classification Tool, both KEGG and GO Terms enrichment analysis of the up-regulated DEGs in iGMSC-D3 also revealed that the top enriched Biological Processes (BPs) and KEGG pathways were linked to lipid/cholesterol metabolic/biosynthetic processes and metabolic pathways (Additional file 2: Figure S3a, c). The enriched Cellular Component (CC) GO Terms included "extracellular exosomes" with 45 enriched genes as presented in the heatmap (Additional file 2: Figure S3b; Additional file 7: Table S6). These results have implicated metabolic reprogramming and increased protein secretion in GMSCs shortly after culturing under the optimized induction culture conditions.

We then further performed gene functional annotation and pathway enrichment analyses of DEGs identified in iGMSC-D6, which were cultured under the optimized induction conditions for another round of 72 h. GSEA analysis revealed that compared to 2D-GMSCs, iGMSC-D6 exhibited enrichment for oxidative phosphorylation (NES: 1.5981114; FDR q-value: 0.0127141), Wnt-β catenin signaling (NES: 1.3766541; FDR q-value: 0.063331), Notch signaling (NES: 1.60066; FDR q-value:

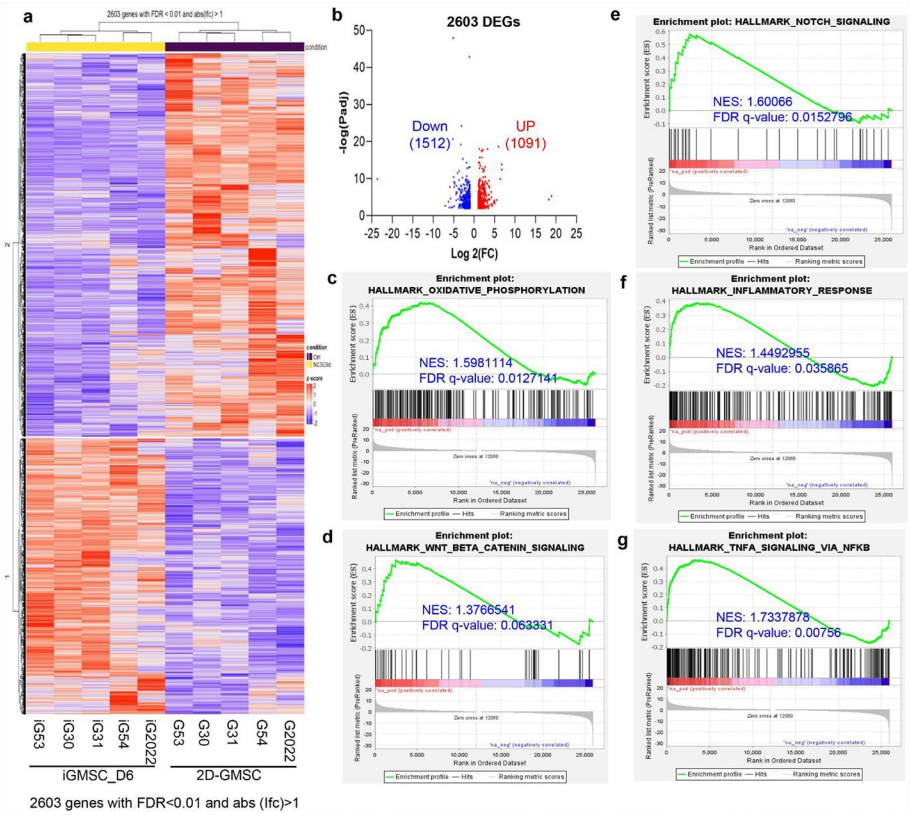

Fig. 1 mRNA sequencing of 2D-GMSCs and iGMSC-D6. mRNA-seq is performed for GMSCs cultured under the defined induction culture conditions for six days (iGMSC-D6) and their 2D-cultured counterparts (2D-GMSCs). **a** Heatmap of differentially expressed genes (DEGs) from mRNA sequencing. FDR < 0.01 and abs(lfc) > 1. n = 5 biological replicates. **b** Volcano plot illustrates the number of significant DEGs between iGMSC-D6 and 2D-GMSCs. Red color symbols represent the upregulated DEGs, while blue symbols represent the downregulated DEGs. (**c-g**) Enrichment plots of gene expression signatures for several signaling hallmarks by gene set enrichment analysis (GSEA) of upregulated DEGs in iGMSC-D6 vs 2D-GMSCs: (**c**) Oxidative phosphorylation; (**d**) Wnt-β-catenin signaling; (**e**) NOTCH signaling; (**f**) Inflammatory response; (**g**) TNF-α signaling via NFκB. NES, normalized enrichment score; FDR, false discovery rate

0.0152796), inflammatory responses (NES: 1.4492955; FDR q-value: 0.035865), and TNFα/NFκB signaling pathway (NES: 1.7337878; FDR q-value: 0.00756) (Fig. 1c-g). According to the DAVID_UniProtKB Keywords (UP_KW) functional annotation analysis of the upregulated DEGs found in iGMSC-D6, the enriched BPs (Biological Processes) include transport, differentiation, lipid metabolism, Wnt signaling pathway, inflammatory responses, angiogenesis, and Notch signaling pathway, while the top enriched CCs (Cellular Components) and MFs (Molecular Functions) include membrane, secreted, cytoplasmic vesicle, and growth factors, etc. (Additional file 2: Figure S4a). Interestingly, there were 124 significantly enriched factors in the secreted category of CCs, including a large panel of growth factors and cytokines, such as *IL-24*, *CHI3L1*, *CSF3*, *BMP2*, *LIF*, *HGF*, *IL-1RN*, *VEGF*, *PTHLH*, *NRG2*, *STC1*, and *TNFAIP6* etc., which have a wide spectrum of biological functions e.g. immunomodulation, wound healing, angiogenesis, and tissue regeneration, etc. (Additional file 2: Figure S4b; Additional file 8: Table S7). According to KEGG pathway and GO Terms enrichment analysis of the upregulated DEGs in iGMSC_D6, the top 30 enriched KEGG pathways include metabolic pathways, cytokine-cytokine receptor, and multiple signaling pathways such as MAPK, Wnt, TGF-β, Hippo, TNFα, and Notch signaling pathways (Additional file 2: Figure S5a). The top 30 enriched GO_BPs and GO_MFs include inflammatory/immune responses, multiple signaling transduction pathways, development, angiogenesis, protein binding, receptor binding and activity, growth factor and cytokine activity, etc. (Additional file 2: Figure S5b, c) The top 30 enriched GO_CCs were linked to cytoplasm and plasma membrane, including extracellular exosomes with a list of 105 related genes (Additional file 2: Figure S5d, e; Additional file 9: Table S8). Altogether, the global transcriptome analysis demonstrated that GMSCs cultured under the optimized induction conditions, especially after the second round 72 h of

culture (iGMSC_D6), underwent drastic alterations in the global gene expression profiles characterized by significant enrichment of signaling pathways and cellular components involved in regulating immunomodulation, metabolism, development, extracellular vesicle/exosome secretion, and angiogenesis, etc., thus endowing them with enhanced pro-regenerative potentials compared to their 2D-GMSC counterparts.

Enhanced secretion of EVs and SPs from iGMSCs cultured under the optimized xeno-free conditions

The above functional gene annotation analysis of the upregulated DEGs found in GMSCs cultured under the optimized xeno-free induction conditions has revealed a significant enrichment in the secreted components and extracellular vesicles (Additional file 2: Figure S3a, b; Figure S4a, b; Figure S5d, e). This prompts us to assess the secretion of EVs and soluble protein factors in the conditioned medium (CM)/secretome of iGMSCs. To this purpose, CMs were harvested from 2D-GMSCs, iGMSC_D3, and iGMSC_D6, respectively, and concentrated by 100 times (100×) using Ultrafiltration units with different MWCF (Molecular Weight Cutt-off) membranes in order to generate concentrated CM fractions containing soluble proteins/peptides with differential molecular weight (kDa) (Fig. 2a). On the one hand, the whole CMs from different culture conditions were subjected to ultrafiltration with a 10 kDa-MWCF to generate the concentrated CM containing soluble protein/peptides with MW > 10 kDa (CM_F1/secretome) (Fig. 2a-①). On the other hand, the whole CMs were subjected to ultrafiltration with a 100 kDa-MWCF to generate the concentrated CM containing soluble protein/peptides with MW > 100 kDa (CM_F2) (Fig. 2a-②), whereby the flow-through were further subjected to ultrafiltration with a 10 kDa-MWCF to generate the concentrated CM containing soluble protein/peptides with 100 kDa > MW > 10 kDa (CM_F3) (Fig. 2a-③).

We then determined the protein concentration of CM_F1/secretome (> 10 kDa) by BCA assay. The results showed that CM_F1/secretome derived from iGMSC_D3 and iGMSC_D6 contains a much higher concentration of proteins than that from a similar number of 2D-GMSCs (Fig. 2b). Western blot analysis revealed that CM_F1/secretome derived from iGMSC_D3 and iGMSC_D6 contains a significant enrichment of several EV markers, including CD9, CD63, CD81, and α-syntenin 1 compared to CM-F1/secretome derived from their 2D-GMSC counterparts (Fig. 2c). Further analysis by Western blotting indicated that CM_F2 (> 100 kDa) and CM-F1/secretome (> 10 kDa) contained similar proteins levels of EV markers but CM-F3 (100 kDa > MW > 10 kDa) were almost depleted of EV markers (Fig. 2d). These

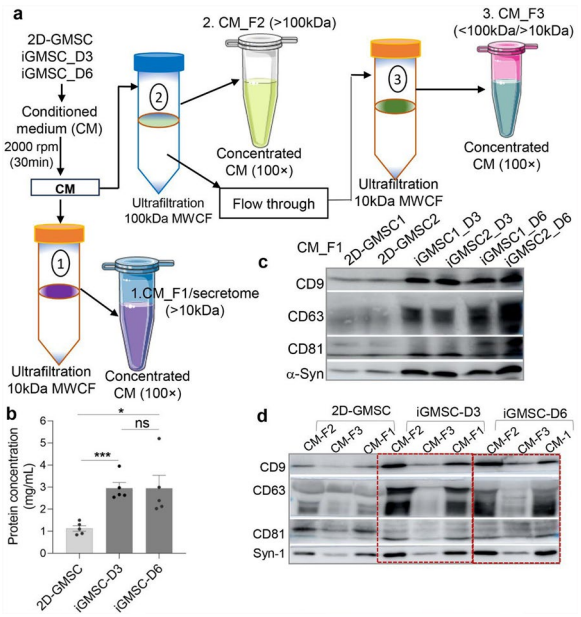

Fig. 2 Enrichment of EVs in the conditioned medium of iGMSCs. Conditioned medium is collected from 2D-GMSCs or GMSCs cultured under the defined induction culture conditions for three days (iGMSC-D3) or six days (iGMSC-D6), which is concentrated 100-fold through ultrafiltration. **a** Schematic illustration of procedures for preparation of different fractions of concentrated CM: CM_F1 containing the whole secretome containing soluble peptides/proteins (SPs) with a molecular weight (MW) > 10 kDa; CM_F2 containing SPs with a molecular weight (MW) > 100 kDa; CM_F3 containing SPs with a MW between 10 and 100 kDa. **b** Protein concentrations (mg/mL) in the whole secretome (CM_F1) are determined by BCA assay. **c** Increased EV marker expressions in the whole secretome of iGMSC-D3 and iGMSC-D6 compared to 2D-GMSCs are determined by Western blot. **d** EVs mainly exist in CM_F1 (the whole secretome) and CM_F2 but not in CM_F3 as determined by Western blot analysis. Data are represented as mean ± SD (n = 5) $*p < 0.05$; $***p < 0.001$; ns, no significance by unpaired *t* test with unpaired two-tailed *t* test with Welch's correction. CM, conditioned culture medium; Syn-1, α-Syntenin1

results suggest that EVs released by GMSCs and iGMSCs exist mainly in CM_F2 with > 100 kDa of MWCF while CM-F1/secretome (> 10 kDa) contain both EVs and SPs.

Separation and characterization of EVs and SPs in the CM/secretome of 2D-GMSCs and iGMSCs

Next, we performed size-exclusion chromatography (SEC) using the qEVoriginal size exclusion columns [33, 36] to separate the EV fractions and SP fractions from the concentrated CM-F1/secretomes derived from 2D-GMSCs and iGMSCs (Fig. 3a). In consistent with previous studies [34], EV particles exist in the 5–8 eluent fractions (F5-F8) with the peak at F6-F7, while the SPs exist in the 17–26 eluent fractions (F17-26) with the peak at eluent fraction 21 (Fig. 3b). The eluent fractions

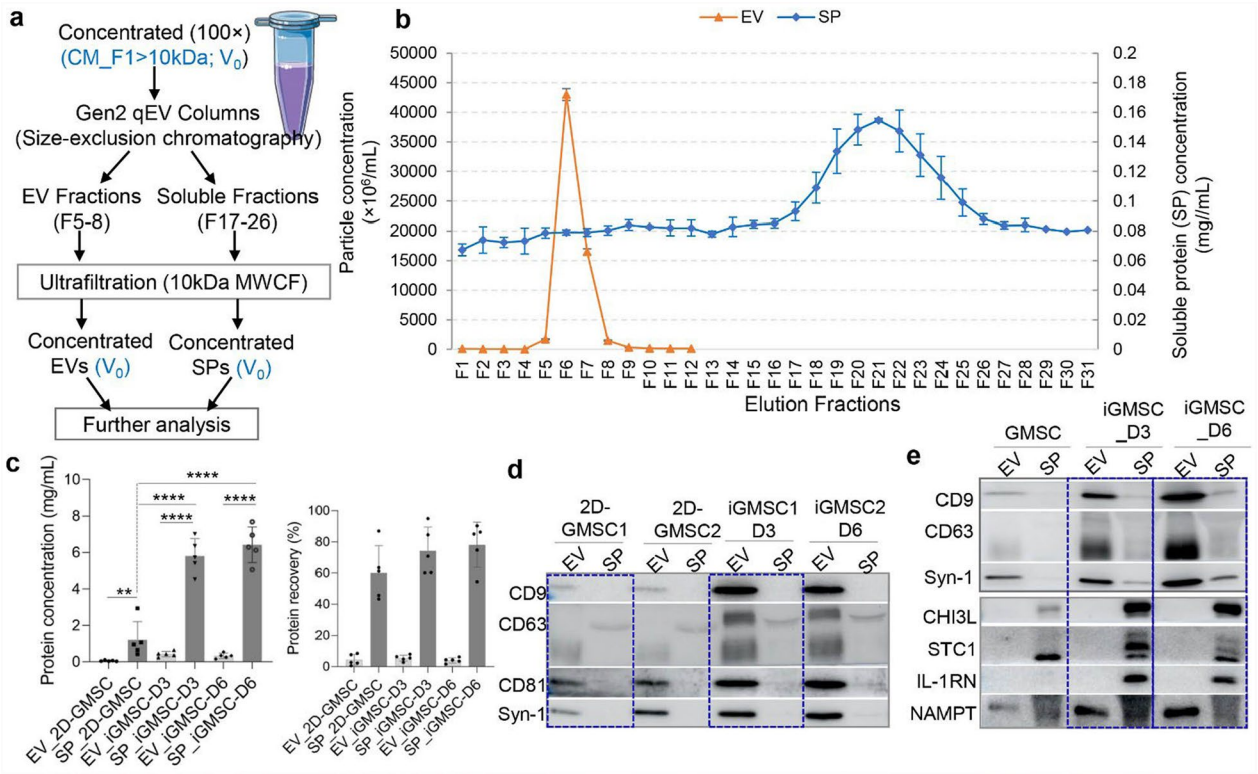

Fig. 3 Molecular characterization of the secretome derived from 2D-GMSCs and iGMSCs. The CM/secretome is prepared by concentrating the culture medium from GMSCs cultured under the defined induction culture condition for three days (iGMSC-D3) or six days (iGMSC-D6) and the 2D-cultured GMSCs through ultrafiltration with a 10 kDa of molecular weight cut-off (MWCO). **a** Schematic illustration of procedures for the separation of extracellular vesicles (EVs) and soluble peptides/proteins (SPs) in the whole CM/secretome (CM_F1) of GMSCs and iGMSCs by using Gen2 qEVOriginal columns (35 nm). CM_F1 at an original volume (V_0) is subjected to elution through qEV column. Both EV and SP elution fractions are combined respectively and concentrated by ultrafiltration to the original volume (V_0) of CM_F1. **b** Distribution of EV particles and SPs in consecutive fractions eluted through the q-EV column. **c** Protein concentrations in separated EV and SP fractions (the left panel) and the recovery rate of SPs following qEV separation (the right panel). **d** The EV markers in the separated EV and SP fractions are determined by Western blot analysis. **e** The level of several secreted proteins in the separated EV and SP fractions are determined by Western blot analysis. Data are represented as mean ± SD (n = 5) $^{**}p < 0.01$; $^{****}p < 0.0001$ by one-way ANOVA with Tukey's multiple comparison test. EV, extracellular vesicle; SP, soluble protein

of EVs or SPs were combined, respectively, and then subjected to ultrafiltration with a 10 kDa-MWCF and concentrated to the original volume (V_0) loaded into the SEC column for separation (Fig. 3a, b). Protein concentration assays revealed a 60 ~ 80% recovery rate of soluble proteins following SEC separation, which exist mainly in the SPs with a very low but detectable level in EVs ($p < 0.0001$ SPs *vs* EVs) (Fig. 3c). Again, the SPs of iGMSCs has a much higher concentration of protein components than those of 2D-GMSC counterparts ($p < 0.0001$) (Fig. 3c). Western blot analysis showed that SP fractions are devoid of EV marker proteins, which only exist in the EV fractions, thus supporting a complete separation of EV fractions with a high purity (Fig. 3d). According to the functional gene annotation analysis of the upregulated DEGs, a large panel of secreted and EV-related components were upregulated transcriptionally in iGMSCs *versus* 2D-GMSC counterparts (Additional file 2: Figure S4a, b; Additional file 2: Figure S5d, e). We then selectively determined the protein secretion of four factors by Western blotting analysis, including CHI3L1 (Chitinase-3-like protein 1), STC1 (Stanniocalcin-1), IL-1RN (the interleukin-1 receptor antagonist), and NAMPT (nicotinamide phosphoribosyltransferase), which have potent immunomodulatory, anti-inflammatory, and pro-regenerative functions under different settings [39–44]. Our results showed that both iGMSC_D3 and iGMSC_D6 secreted a much higher level of these protein factors than their 2D-GMSC counterparts (Fig. 3e). Interestingly, it was noted that CHI3L1, STC1, and IL-1RN proteins existed only in the SPs, whereas NAMPT protein existed in both EV and SP fractions (Fig. 3e). These results have confirmed the significantly enhanced secretion of SPs independent of EVs by iGMSCs compared to their 2D-GMSC counterparts.

Next, nanoparticle tracking analysis (NTA) with ZetaView was performed to further characterize EVs secreted by 2D-GMSCs and iGMSCs. The results showed that EVs secreted by 2D-GMSCs and iGMSCs have a similar size distribution, with an average size of 169.33 ± 22.99 nm, 153.59 ± 11.66 nm, and 155.78 ± 7.68 nm for EVs derived from 2D-GMSC, iGMSC_D3, and iGMSC_D6 ($p > 0.05$), respectively

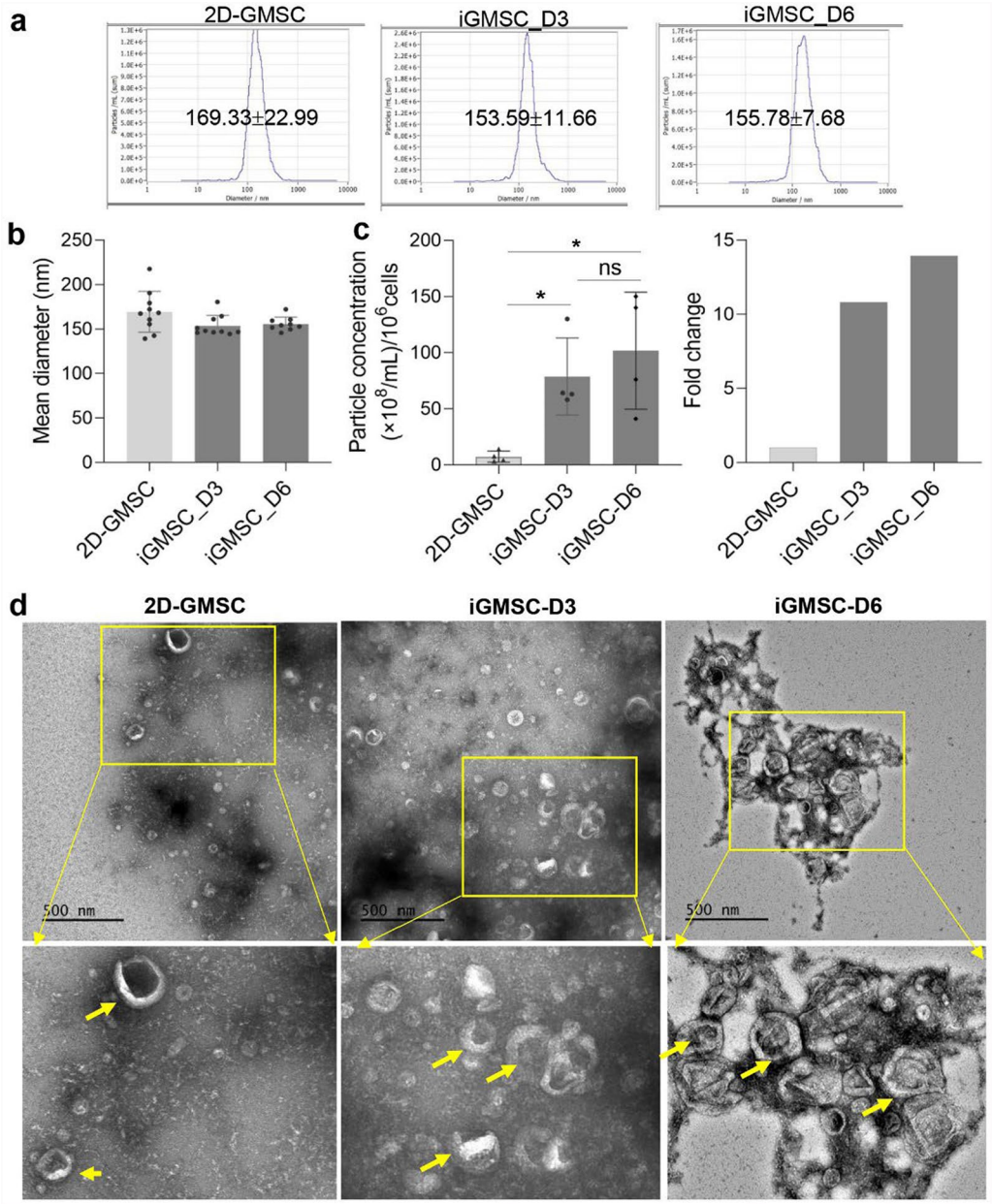

Fig. 4 Size distribution and morphological characterization of purified EVs derived from 2D-GMSCs and iGMSCs. The CM/secretome is prepared by concentrating the culture medium from GMSCs cultured under the defined induction culture condition for three days (iGMSC-D3) or six days (iGMSC-D6) and the 2D-cultured GMSCs through ultrafiltration with a 10 kDa of molecular weight cut-off (MWCO). **a** The size distribution and concentration of EVs purified from the concentrated conditioned medium (CM)/secretome of 2D-GMSCs and iGMSCs are determined by ZetaView Nanoparticle Tracking Analysis (NTA) instrument. Representative spectra are shown. **b** The mean of particle diameter size (nm) of purified EVs is shown in the graphs. **c** The mean of particle concentration (particle number/mL) and fold change (relative to 2D-GMSCs) of purified EVs are shown in the graphs. **d** TEM visualization of purified EVs. Scale bars in 500 nm are shown in the upper panels of images. Lower panels represent the enlargement of the circled areas from the corresponding upper panel of image. Data are represented as mean ± SD *$p < 0.05$; ns, no significance by one-way ANOVA with Tukey's multiple comparison test

(Fig. 4a, b). TEM images confirmed that the purified EVs were exosome-sized, cup-shaped vesicles (Fig. 4d). In consistent with Western blot analysis, NTA revealed an over tenfold increase in the EV yield (EV particles/10^6 cells/mL) secreted by iGMSC_D3 and iGMSC_D6 *versus* their 2D-GMSC counterparts (Fig. 4c). These results further confirmed the enhanced EV secretion by GMSCs cultured under the optimized induction culture conditions.

Functional analysis of the CM/secretome derived from 2D-GMSCs and iGMSCs: effects on macrophages and skeletal muscle progenitor cells

Numerous studies have shown that MSC-derived secretomes exert therapeutic effects on immune/inflammatory diseases and wound healing by promoting the polarization of anti-inflammatory M2 macrophages [45]. Herein, we showed that cultured Raw264 murine macrophages could uptake the PKH26-prelabeled EVs when exposed to the CM/secretome of 2D-GMSCs and iGMSCs (Additional file 2: Figure S6a, b). ELISA assays showed that stimulation of Raw 264 macrophages with the CM/secretome of 2D-GMSCs, iGMSC_D3, and iGMSC_D6 led to a dose-dependent increase in the secretion of IL-10 ($p < 0.001$), a signature anti-inflammatory cytokine produced by M2 macrophages, whereby the stimulatory effect conferred by the CM/secretome of iGMSC_D3 and iGMSC_D6 was more pronounced than that of 2D-GMSCs (Additional file 2: Figure S6c, d). Further analysis of the ELISA results indicated that the secretome of iGMSC_D6 had stronger stimulatory effect on IL-10 secretion by macrophages than that of iGMSC_D3 (Additional file 2: Figure S6e). On the other hand, treatment with the CM/secretome of 2D-GMSCs, iGMSC_D3, and iGMSC_D6 led to a dose-dependent decrease in LPS-stimulated TNF-α secretion by Raw264 macrophages (Additional file 2: Figure S6f, g), whereby the suppressive effect mediated by CM/secretome of iGMSC_D6 on LPS-stimulated TNF-α secretion is comparable to iGMSC_D3 but stronger than that of 2D-GMSCs (Additional file 2: Figure S6g, h). These results demonstrated that the CM/secretome of iGMSCs has enhanced stimulatory effect on M2 macrophage polarization and enhanced inhibitory effect on LPS-stimulated M1 macrophage activation compared to that of 2D-GMSC counterparts. The following functional analysis focused on the CM/secretome of iGMSC_D6 compared to that of 2D-GMSC counterparts.

Given the critical role of skeletal muscle satellite cells (SkMuSCs) in the homeostasis and regeneration of skeletal muscle, we then explored whether the CM/secretome derived from 2D-GMSCs and iGMSCs had any direct effects on SkMuSCs other than macrophages. We initially

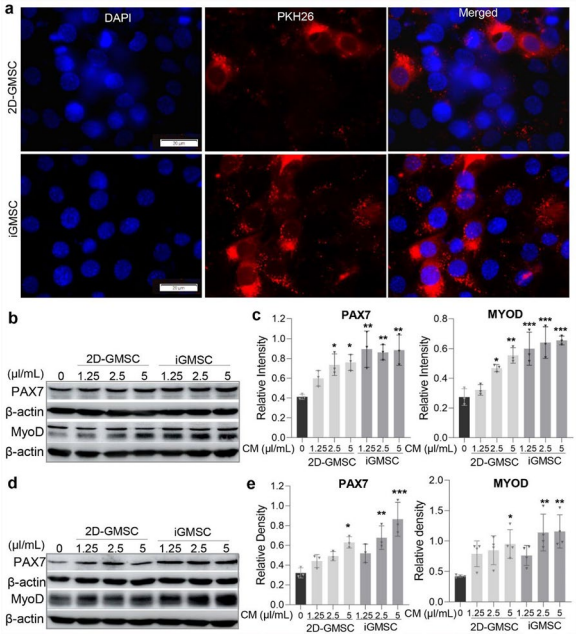

Fig. 5 Effects of CM/secretome derived from 2D-GMSCs and iGMSCs on myogenic gene expressions in skeletal muscle progenitors. The CM/secretome is prepared by concentrating the culture medium from GMSCs cultured under the defined induction culture condition for six days (iGMSC) and 2D-cultured GMSCs through ultrafiltration with a 10 kDa of molecular weight cut-off (MWCO). **a** Uptake of PKH26-labeled EVs by C2C12 myoblasts. The prepared CM/secretome is pre-labelled with PKH26. C2C12 myoblasts are incubated with 10 μg/mL of PKH26-prelabelled CM/secretome for 24 h. Cells are observed under a fluorescence microscope. The nuclei are stained with DAPI (4′,6-diamidino-2-phenylindole). Scale bar, 20 μm. **b, c** C2C12 myoblasts are incubated in the presence or absence of different volume of the CM/secretome (1.25, 2.5, 5 μl/mL) of 2D-GMSC and iGMSC for 48 h. The expression of PAX7 and MYOD is determined by Western blot. **d, e** Human skeletal muscle progenitor cells are incubated in the presence or absence of different volume of CM/secretome (1.25, 2.5, 5 μl/mL) of 2D-GMSC and iGMSC for 48 h. The expression of PAX7 and MYOD is determined by Western blot. (c, e) Semi-quantification of the protein band density by using Image J is shown as a ratio of PAX7 and MYOD to β-actin as the internal control. Data are represented as mean ± SD (n = 3). *$p < 0.05$; **$p < 0.01$; ***$p < 0.001$ compared with the control by one-way ANOVA with Tukey's multiple comparison test. CM, conditioned culture medium

observed that C2C12 cells, a murine-derived myoblast cell line as a well-recognized platform in the field of muscle biology and regeneration, efficiently uptake PKH26-prelabled EVs in the CM/secretome of both 2D-GMSCs and iGMSCs (Fig. 5a). Western blot results showed that stimulation of C2C12 cells with the CM/secretome of 2D-GMSCs and iGMSCs dose-dependently promoted the protein expression of PAX7 and MyoD, two key myogenic transcriptional factors that govern the self-renewal and early activation of SkMuSCs [46], whereby

iGMSC-derived CM/secretome had stronger inductive effects on PAX7 and MyoD expression than 2D-GMSC-derived CM/secretome (Fig. 5b, c). The robust inductive effect of iGMSC-derived CM/secretome versus 2D-GMSC-derived CM/secretome on PAX7 and MyoD expressions was further confirmed in human SkMuSCs as determined by Western blot analysis (Fig. 5d, e). These results demonstrated that iGMSC-derived CM/secretome exerted enhanced pro-myogenic potentials compared to that derived from 2D-GMSCs.

iGMSC-derived CM/secretome enhanced skeletal muscle regeneration in a rat tongue defect model

Given that iGMSC-derived CM/secretome enhanced the expression of key myogenic factors in SkMuSCs and M2 macrophage polarization that play important multifaced roles in the homeostasis and repair/regeneration of injured skeletal muscles [47], we then explored the regenerative and therapeutic potentials of the CM/secretome derived from 2D-GMSCs (2D-GMSC-CM) and iGMSC (iGMSC-CM) in a rat tongue defect model [20, 21]. Six weeks post-surgery, clinical morphological examination showed that the wounded tongue of rats treated with 2D-GMSC-CM or iGMSC-CM exhibited less contraction and maintained the overall tongue shape without deformity compared to the SIS/Fibrin and SIS alone control groups (Fig. 6a). Histological analysis revealed that both 2D-GMSC-CM and iGMSC-CM groups showed better or improved re-epithelialization as evidenced by complete restoration of keratinized tissues and more regularly arranged papillae in comparison with the SIS/Fibrin and SIS alone control groups (Fig. 6b). Desmin is an intermediate filament protein highly expressed in immature, newly regenerated myofibers, including in tongue muscles [48]. Immunofluorescence staining showed a remarkable increase in the expression of desmin protein in the injured tongue muscle layers of rats from both 2D-GMSC-CM and iGMSC-CM groups compared to the SIS/Fibrin and SIS alone control groups, but the increase in desmin expression in iGMSC-CM group was significantly more pronounced than that in the 2D-GMSC-CM group ($p < 0.05$) (Fig. 7a-c). Collectively, these results demonstrated that iGMSC-derived CM/secretome possesses enhanced potential to facilitate epithelial and muscle regeneration of injured rat tongue in comparison with 2D-GMSC-derived CM/secretome.

We then examined the effect of the CM/secretome of GMSCs and iGMSCs on the infiltration and polarization of macrophages in rat tongue defects. At six weeks post-surgery, there was still noticeable infiltration of $CD68^+$ macrophages in the wounded area of rat tongues from the SIS/Fibrin and SIS alone control groups, which was significantly attenuated following treatment with 2D-GMSC-CM and iGMSC-CM ($p < 0.001$). Of note, iGMSC-CM exhibited stronger inhibitory effect on macrophage infiltration than 2D-GMSC-CM (Additional file 2: Figure S7). In addition, our results showed that treatment with 2D-GMSC-CM and iGMSC-CM

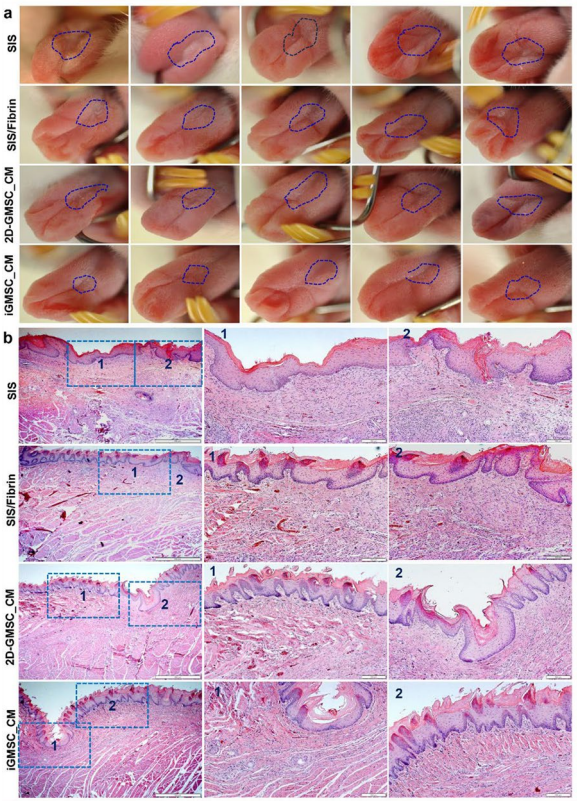

Fig. 6 Integration of SIS-ECM membrane and fibrin sealant mixed with iGMSC-CM/secretome promotes the healing of rat tongue defects. The CM/secretome is prepared by concentrating the culture medium from GMSCs cultured under the defined induction culture condition for six days (iGMSC) and 2D-cultured GMSCs through ultrafiltration with a 10 kDa of molecular weight cut-off (MWCO). 30 µl of Tisseel fibrin sealant (Fibrin) mixed with 50 µg of 2D-GMSC-CM or iGMSC-CM is applied to the rat tongue defect and covered with a strip of porcine small intestine submucosal (SIS) matrix membrane. **a** Rat tongues were photographed six weeks after the surgery. Blue circles indicate the area of the defect post-surgery. **b** The corresponding H & E staining of cross sections of tongue specimens from different groups of rats six weeks post-surgery. The middle and right panels show the enlargement of the corresponding circled fields in the left panels. Scale bars, 200 µm (the left panels) and 100 µm (the middle and right panels). SIS, rat tongue defects treated with porcine small intestine submucosal matrix alone; SIS/Fibrin, rat tongue defects treated with SIS in combination with Tisseel fibrin sealant; 2D-GMSC-CM, rat tongue defects treated with SIS/Fibrin in combination with the CM/secretome from 2D cultured GMSCs; iGMSC-CM, rat tongue defects treated with SIS/Fibrin in combination with the CM/secretome from iGMSCs. SIS, small intestine submucosa; CM, conditioned culture medium

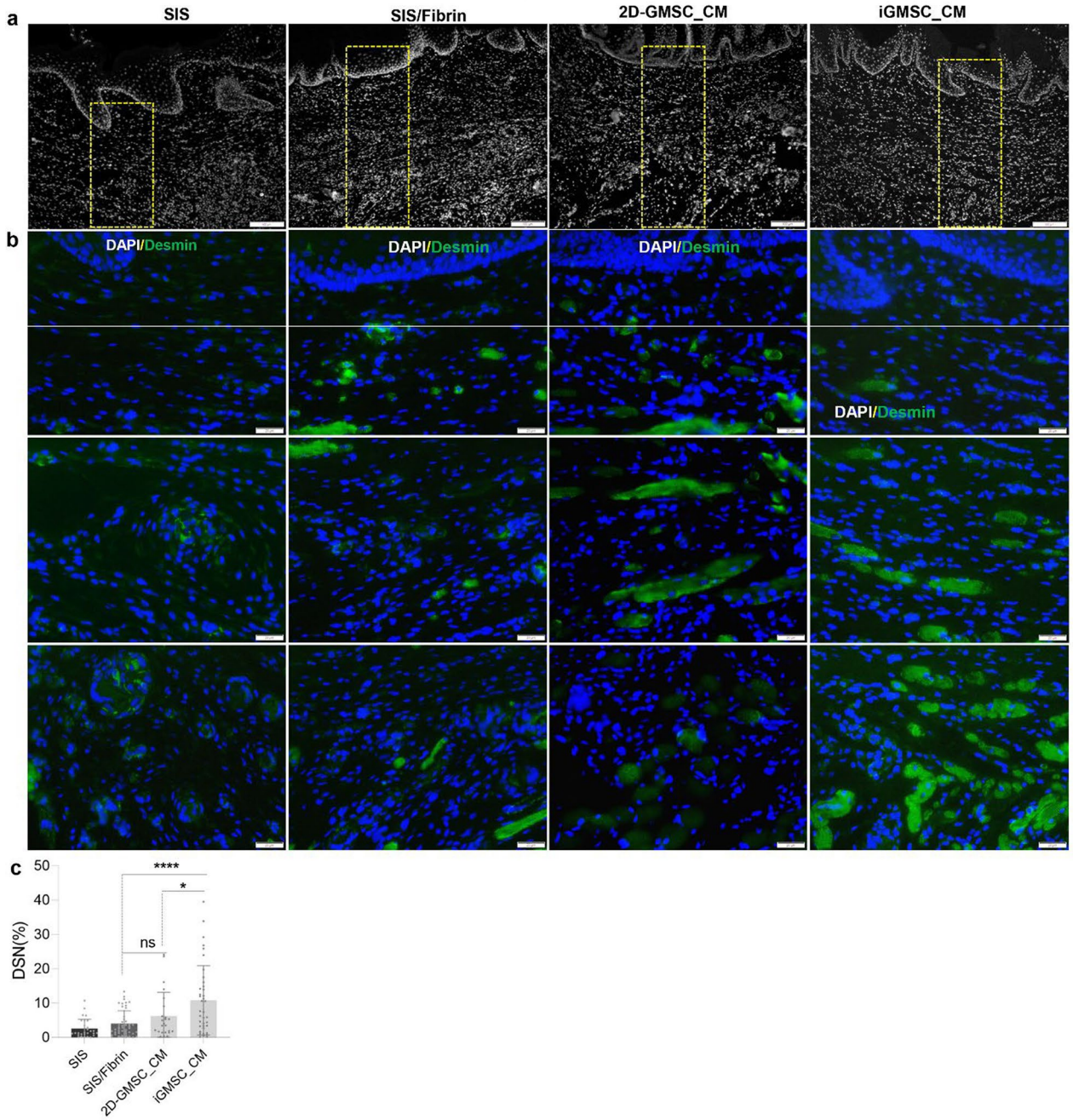

Fig. 7 Local application of iGMSC-secretome promotes rat tongue muscle regeneration. Six weeks post-surgery, rat tongue tissues from different treatment groups were harvested and 10 µm-thick cryosections were cut for immunostaining of desmin (DSN) expression. **a** The grayscale images show the nuclei stained with DAPI (4′,6-diamidino-2-phenylindole) at a lower magnification. Scale bar, 100 µm. **b** Cryosections are immune-stained with a primary antibody for desmin followed by staining with Alexa Fluor-488 conjugated secondary antibody. The nuclei are stained with DAPI. Images are captured under a fluorescence microscope. Scale bar, 20 µm. **c** Quantification of the fluorescence intensity of desmin (green) using Image J. Data are represented as mean ± SD. *$p < 0.05$; ****$p < 0.0001$; ns, no significance by one-way ANOVA with Tukey's multiple comparison test. SIS, small intestine submucosa; CM, conditioned culture medium

significantly increased the infiltration of M2 macrophages characterized by the increased expression of arginase-1 ($CD68^{+}Arg1^{+}$ macrophages) compared with the SIS/Fibrin or SIS alone control ($p < 0.001$), whereby iGMSC-CM exhibited a relatively stronger stimulatory

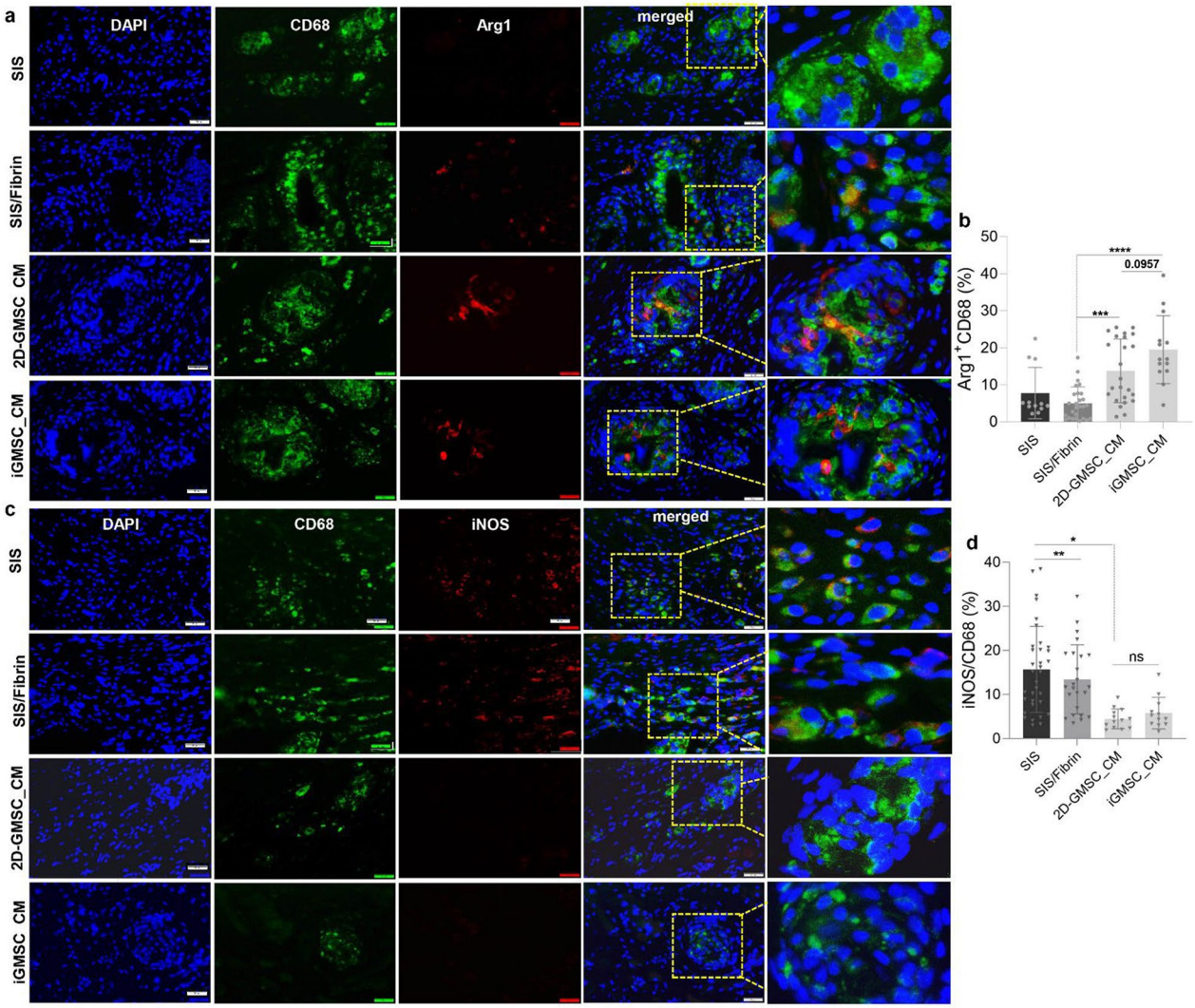

Fig. 8 Effects of GMSC-secretome on macrophage polarization in rat tongue defects. Six weeks post-surgery, rat tongue tissues from different treatment groups were harvested and 10 µm-thick cryosections were cut for immunostaining of M1 and M2 macrophage markers. **a** Cryosections are immune-stained with a primary antibody for CD68 and Arginase-1 (Arg-1) followed by staining with corresponding Alexa Fluor-488 and Alexa Fluor-594 conjugated secondary antibodies, respectively. CD68, green color; Arg-1, red color. The nuclei are stained with DAPI. Images are captured under a fluorescence microscope. Scale bar, 20 µm. The far-right panels represent the enlarged images of the squared areas in the panel of merged images. **b** Quantification of the co-localization of Arg-1 and CD68 using Image J. **c** Cryosections are immune-stained with a primary antibody for CD68 and inducible nitric oxide synthase (iNOS), followed by staining with the corresponding Alexa Fluor-488 and Alexa Fluor-594 conjugated secondary antibodies, respectively. CD68, green color; iNOS, red color. The nuclei are stained with DAPI. Images are captured under a fluorescence microscope. Scale bar, 20 µm. The far-right panels represent the enlarged images of the squared areas in the panel of merged images. **d** Quantification of the co-localization of iNOS and CD68 using Image J. Data are represented as mean ± SD. *$p < 0.05$; **$p < 0.01$; ***$p < 0.001$; ****$p < 0.0001$; ns, no significance by one-way ANOVA with Tukey's multiple comparison test. SIS, small intestine submucosa; CM, conditioned culture medium

effect on M2 macrophage infiltration than 2D-GMSC-CM (p = 0.0957) (Fig. 8a, b). On the other hand, compared with the SIS/Fibrin or SIS alone control, 2D-GMSC-CM and iGMSC-CM exhibited comparable inhibitory effect on the infiltration of M1 macrophages characterized by the decreased expression of iNOS ($CD68^+iNOS^+$ macrophages; $p < 0.05$) (Fig. 8c, d). Collectively, these results suggest that iGMSC-derived CM/secretome possess relatively stronger in vivo anti-inflammatory effect than that derived from 2D-GMSCs through modulating the infiltration and polarization of macrophages, particularly through promoting M2

macrophage polarization, potentially contributing to tongue muscle regeneration of rats.

Discussion

It is increasingly recognized that MSCs primarily exert their therapeutic and regenerative effects through their paracrine secretome, which contains EVs and various EV-independent bioactive factors [3, 8, 11, 12]. This had laid the foundation for the potential application of exogenous MSC-derived cell-free products, either the whole secretome, purified EVs, or EV-free soluble factors as the alternative therapeutics in tissue engineering and regenerative medicine (TE/RM) [3, 12, 13, 49]. Even though many preclinical studies have demonstrated the replicative efficacy and the advantages of MSC-derived EVs/exosomes *versus* the parental MSCs in the treatment of a broad spectrum of human disease models [14], there is still lack of promising outcomes from a limited number of clinical trials that directly use MSC-derived EVs/exosomes as therapeutics for human diseases [16]. This might be, at least in part, due to the fact that EVs only partially represent the biological functions of the whole secretome of MSCs since an increasing number of studies have shown that EV-independent bioactive soluble factors in the secretome had synergistical therapeutic effects with EVs [12]. For instance, a recent study showed that BMSC-derived conditioned medium (CM) has stronger suppressive effect on inflammation in tenocytes than its EV faction, suggesting the superior therapeutic efficacy of the whole CM compared with the purified EV fraction alone in the treatment of tendon injuries [50]. In a mouse model of acute skeletal muscle injury, it has been shown that EVs and soluble factors in ADSC-derived CM/secretome act synergistically to facilitate muscle regeneration [51]. Further comparison studies indicate that ADSC-derived whole CM/secretome has stronger protective effect against cellular senescence while only EVs exhibited anti-inflammation effect [51]. In addition, previous studies have shown that whole CM derived from BMSCs and ADSCs also displayed superior anti-inflammatory effects and MMP inhibitory effect in comparison with its EV and soluble protein fractions in an in vitro OA model and inflamed nucleus pulposus and annulus fibrosus cell model [52–54]. Most recently, Papait A et al. have compared the immunomodulatory effects of the total secretome, EVs, and EV-free fractions derived from human amniotic mesenchymal stromal cells (hAMSCs) on both innate and adaptive immune cells. Their results demonstrate that the immunomodulatory functions of hAMSC-derived secretome are attributed to soluble factors (SFs) but not purified EVs when tested at original concentrations [35]. Collectively, these studies support the superiority of the whole MSC-derived CM/secretome over its EV or SF fraction alone as the cell-free therapeutic products in disease treatment because of the maximal therapeutic potential of the whole secretome of MSCs, as well as the elimination of the additional downstream steps in manufacturing therapeutic EV products [12, 55, 56]. In the present study, we demonstrated that local application of iGMSC-derived CM/secretome loaded with the commercially available SIS membrane and fibrin sealant remarkably facilitated re-epithelialization and muscle regeneration in a rat tongue defect model (Fig. 6 and Fig. 7), thus highlighting the potential application of iGMSC-derived CM/secretome in tissue engineering and regenerative medicine (TE/RM).

Even though mounting pre- and clinical studies have established the safety profile of MSCs and their derivative secretomes/EVs in the regenerative therapies of various pathological conditions, large variations or inconsistencies exist in the reported clinical outcomes. These challenges might be attributed to the inherent heterogeneity of MSCs and their derivative secretomes/EVs associated with diverse intrinsic and extrinsic factors in both the upstream and downstream manufacturing processes of MSC/secretome products, including the age and health conditions of donors, the source of tissues, states of tissue harvest (e.g. storage, transport, processing), and variable conditions for cell isolation/culture and secretome/EV preparation, the administration of MSC-derived cell-free products (e.g. the route, dosage, and frequency), as well as the health status of the recipients [7, 56–59]. To date, different strategies, both genetic modification and nongenetic approaches, have been implemented to re-educate or license exogenous MSCs, aiming to optimize their properties and functions, and consequently, improving their therapeutic efficacy in different clinical settings [11, 49, 59]. Among the nongenetic approaches, hypoxic culture, preconditioning with pro-inflammatory cytokines, biomaterials, and three-dimensional (3D) culture, are among the most common approaches to generate predictable and reliable therapeutic MSC-derived cell-free products, e.g. secretomes and EVs, with improved immunomodulatory and regenerative potentials of MSCs [49, 55, 60]. Given that GMSCs represent a unique subpopulation of neural crest-derived MSCs [61, 62], our recent studies have shown that GMSCs cultured under defined culture conditions, including in specialized 3D-collagen hydrogel with optimal stiffness, readily converted into neural crest stem-like cells with enhanced capabilities to promote nerve regeneration [22, 23, 63]. In the present study, we reported that GMSCs cultured under the optimized xeno-free induction conditions (iGMSCs) *versus* the standard serum-free 2D-cultures (2D-GMSCs) showed significant transcriptome changes

characterized by the transcriptional upregulation of differentially expressed genes (DEGs) which are functionally enriched in fatty acid metabolism, oxidative phosphorylation, Notch and Wnt signaling pathways, inflammatory responses, secretion and exosome biogenesis (Fig. 1; Additional file 2: Figure S4, S5). Importantly, there is about a normalized threefold increase in the protein content and a normalized tenfold increase in EV particles in iGMSC-derived CM/secretome compared to that derived from 2D-GMSCs (Fig. 2, Fig. 4). These compelling results have highlighted the feasibility of improving the intrinsic property of GMSCs through optimizing the culture conditions, and consequently, augmented their secretion profile with enriched EVs and bioactive soluble protein (SP) factors.

Due to the complex components of MSC-derived secretome and EV cargos, it is rationalized that MSC-based products exert the therapeutic and regenerative effects through multiple mechanisms of action[60], among which the potent immunomodulatory/anti-inflammatory functions of MSC-derived secretome and EVs, especially their promotive effects on the polarization of anti-inflammatory M2 macrophages as well as their inhibitory effects on the activation of pro-inflammatory M1 macrophages[64, 65], might contribute a major part to their therapeutic and regenerative potency. Of note, several studies have identified the unique profiles of soluble factors and exosomal miRNAs in MSC-derived secretome that are linked to the immunomodulatory functions on macrophages under different inflammatory settings[65–68]. In the present study, we demonstrated that iGMSC-derived CM/secretome enriched with EVs and SPs has enhanced promotive effective on M2 macrophage polarization compared with 2D GMSC-derived CM/secretome both in vitro (Additional file 2: Figure S6) and in vivo using a rat tongue defect model (Fig. 8). According to the mRNA-seq results, we confirmed the increased secretion of three representative EV-free soluble protein factors including CHI3L1, STC1, and IL-1RN, and one representative factor, NAMPT, which exists simultaneously in and outside EVs (Fig. 3). Previous studies have shown that CHI3L1 [39], STC1[40, 41], IL-1RN[42], and NAMPT[44] individually have multifaced roles in MSC-mediated immunomodulation, anti-inflammation, angiogenesis, and anti-senescence that are beneficial to tissue regeneration. For instance, a recent study has reported that MSCs alleviate experimental immune-mediated liver injury via CHI3L1-mediated T cell suppression [39], while CHI3L1 has also been shown to promote angiogenesis and M2 macrophage polarization in choroidal neovascularization development [69]. Oh JY et al. has reported that hMSCs decrease mitochondrial ROS and inhibit NLRP3 inflammasome activation in macrophages primarily by secreting STC-1 [70], while STC-1 secreted by human umbilical mesenchymal stem cells promotes IL-10 expression in alveolar macrophages [41]. IL-1RN is another important MSC-derived anti-inflammatory mediators by suppressing macrophage-driven inflammation [42, 71]. Lee et al. has reported that MSCs promote M2 macrophage polarization in an IL-1RN-dependent manner, which contributes to MSC-mediated alleviation of acute liver failure [72]. Regarding the role of NAMPT in MSC-mediated therapeutic effects, a recent study has shown that NAMPT encapsulated in young adipose-derived mesenchymal stem cells (ADMSCs)-derived EVs plays an important role in ADMSC-mediated therapeutic effect on tendinopathy in a "One-Stone-Two-Birds" manner [44]. They have further shown that young ADMSC-derived EVs exert anti-senescent effect on tenocytes through the NAMPT/SIRT1/PPARγ/PGC-1α pathway, and concomitantly, promote phagocytosis and M2 polarization through the NAMPT/SIRT1/Nf-κb p65/NLRP3 pathway [44]. Given that these factors play important roles in MSC-mediated anti-inflammatory and regenerative functions and are significantly increased in the secretome of iGMSCs, it is warranted to perform further studies with genetic approaches, e.g. siRNA/shRNA or CRISPR gene editing approaches to knockdown or knockout their expressions in GMSCs to confirm whether these factors contribute individually or synergistically to the enhanced immunomodulatory and therapeutic effects of iGMSC-derived secretome both in vitro and in vivo.

Up to date, numerous studies have implicated the important role of endogenous MSCs in skeletal muscle development, homeostasis, regeneration, aging, and diseases [73] as well as the potential application of exogenous MSCs and their derivative cell-free products in tissue engineering and regenerative therapy of injured and dystrophic skeletal muscles [74]. For instance, a recent study has shown that the conditioned media (CM) and EVs derived from mesenchymal stromal cells from the amniotic membrane (hAMSCs) promote dystrophic muscle regeneration by supporting proliferation and differentiation of resident MuSCs and inhibiting fibrosis and MuSC exhaustion [75]. In addition, Mitchell R et al. has reported that EVs and soluble factors in ADSC-derived CM/secretome act synergistically to facilitate muscle regeneration through CM/secretome-mediated anti-senescence and EV-mediated anti-inflammatory effect [51]. However, it is noteworthy that most of the current studies on stem cells and skeletal muscle regeneration focused on limb muscles, while the intrinsic regenerative potential as well as the potential application of stem cell-based tissue engineering and regenerative therapy of the skeletal muscle of tongue as a vital organ with specialized

functions in speaking and eating has been insufficiently investigated [48, 76]. In the present study, we demonstrated that iGMSC-derived CM/secretome upregulated the expression of the key myogenic transcription factors, PAX7 and MyoD, in cultured SkMuSCs, and remarkably enhanced muscle regeneration in a rat tongue defect model (Fig. 6, Fig. 7). Given that iGMSC-derived CM/secretome also promote M2 macrophage polarization during regeneration of rat tongue muscle defects, it is plausible that iGMSC-derived CM/secretome promotes tongue muscle regeneration through simultaneously promoting M2 macrophage polarization and SkMuSC activity. However, further studies are warranted to identify the bioactive soluble factors and/or components of EV cargos that contribute either distinctively or synergistically to the immunomodulatory and myogenic effects of iGMSC-derived secretome both in vitro and in vivo, and to explore whether iGMSC-derived secretome has enhanced therapeutic effect on regeneration of other types of skeletal muscles.

Challenges and limitations

It is noteworthy that there are several limitations in this study and some common challenges in translating MSC-based cell-free therapies to clinical settings. One of the major concerns is the lack of a standard protocol for both upstream (MSC isolation, expansion, storage) and downstream (bioprocessing of secretome/EVs products) procedures to generate the final cell-free products [12, 56]. In this study, we optimized the xeno-free induction medium first reported in our previous protocol [22] by minimizing the use of nutritional supplement, growth factors and small molecules, including transferrin-depleted N2 supplement, EGF, bFGF, a small molecule inhibitor of TGFβR (SB431542). Through the concentration and washing steps using the ultrafiltration unit with 10-kDa MWCO membranes, it is expected to remove most of the supplemental components and minimize the effect of the residual carryover of these supplements on the quality and bioactivity of the final iGMSC-derived secretome products. However, further studies are necessary to rule out the contaminating effects of the potential remnants of the supplemental components in the culture media.

It is known that characteristics of donors (e.g. age and healthy status), tissue origins, and cell passages have significant effects on the components and bioactivities of MSC-derived secretome/EV products [12, 77]. Regarding the effects of tissue sources on MSC-derived secretome/EVs, a recent study performed proteomic profiling analyses and identified different protein profiles in the secretomes derived from bone-marrow (BMMSCs), umbilical-cord (UCMSCs), adipose-tissue (ATMSCs) and clinical/commercial-grade induced pluripotent stem cell-derived MSCs (iMSCs) under resting and inflammatory licenced conditions [78]. To minimize the effect of donor age and cell passages, this study used GMSCs derived from healthy donors aged from 20–40 years old with less than sixth passages. However, further studies are necessary to extend our current findings by including GMSCs derived from older patients and other sources of MSCs, such as ADSCs and BMMSC, and UCMSCs, to validate whether our current xeno-free induction conditions can also improve secretome production with enriched EVs and SPs.

As mentioned above, MSC-derived secretomes contain complex components including growth factors, cytokines, lipids, RNAs (especially miRNAs), which are either encapsulated inside exosomes/EVs or exist independently as EV-free soluble factors[3, 12, 77]. Therefore, it remains one of the major challenges to profile complex molecules and identify the distinctive bioactive factors that contribute to MSC-secretome/EV-mediated therapeutic effects under different disease settings. In this study, we showed a significant enrichment of EVs and several soluble protein (SPs) factors in iGMSC-derived CM/secretome, but it is necessary to perform proteomics, miRNA sequencing, and lipidomics to comprehensively profile the complex bioactive molecules in iGMSC-derived CM/secretome and purified EVs, which can help to identify the major bioactive components that contribute individually or synergistically to iGMSC-derived CM/secretome mediated immunomodulatory and myogenic functions both in vitro and in vivo.

From the standpoint of clinical application, the final MSC-derived secretome/EV product should be appropriately formulated and stored until the use to maintain the quantity and biological activity of the bioactive molecules [12]. To date, there is still a lack of standard protocols for the preparation, formulation, and storage of MSC-derived secretome/EV products, but generally, it is recommended that MSC-derived secretome/EV products are lyophilized and stored at −80 °C for long-term use purposes [7, 13]. In this study, we routinely stored aliquots of GMSC-derived CM/secretomes, EVs, and SP products at −80 °C. However, further studies are necessary to evaluate changes in the contents (EVs and SPs), the immunomodulatory and myogenic functions of iGMSC-derived CM/secretome following storage at −80 °C for different time periods.

Another challenge facing this field is the lack of the consensus for dose, frequency, and route of administration as well as for biodistribution analysis of MSC-derived secretome/EVs. For instance, variable units, including microgram (μg) based on the protein content, the particle number (EVs), and volume (μl), have been utilized for dosing MSC-derived secretome/EV products

with a large variation in the range of dosages for different sources of secretome/EVs and disease conditions [12, 77]. In addition, there is no standard protocol for assessment of the biodistribution of MSC-derived secretome/EVs because of the reported short half-life of EVs and soluble factors in the secretome when administered systemically [79]. For the local application, different types of biomimetic scaffolds/hydrogels are loaded with MSC-derived secretome/EVs, allowing a sustained and controllable delivery and delayed degradation, thus improve the therapeutic effectiveness [80]. In this study, we mixed iGMSC-derived CM/secretome at a dosage of 50 μg in term of protein content with clinical-grade Tisseel Fibrin Glue and locally applied to the tongue defect. However, further studies are necessary to optimize the dosage and assess the biodistribution and retention of iGMSC-secretome in the local tongue defect areas by pre-labeling EVs with appropriate fluorescence dyes.

Even though numerous preclinical and clinical studies have demonstrated the biosafety and potency of MSC-derived secretome/EV products in treating various diseases [3, 7], their safety and efficacy should be ensured before translation into clinical use. Generally, the biosafety assessments of MSC-derived secretome/EV products, especially for the use of allogeneic MSC-derived products, should include pharmacokinetics and pharmacodynamic analysis, immunogenicity, biocompatibility, and overall safety such as the risk of microbial, mycoplasma and/or viral contamination, and the level of endotoxin [12]. Given the potent anti-inflammatory and pro-angiogenic activities of MSC-derived secretome/EVs, caution measures should be considered given their long-term use may result in immunosuppression, risk of infection and tumor growth [81]. Therefore, it is necessary to conduct a long-term follow-up (e. g. 12 weeks or more) study to determine whether iGMSC-secretome/EV-mediated regeneration of rat tongue muscle maintains its structural and functional integrity over time and to assess the durability of iGMSC-secretome/EV-mediated therapeutic effects and potential long-term safety issues in the rat tongue defect model.

Conclusion

In summary, our present study has demonstrated that GMSCs cultured under the optimized xeno-free induction conditions, designated as iGMSCs, had significant changes in the global gene expression profiles characterized by a significant upregulation of a large panel of genes related to EVs and secreted factors compared to their 2D-cultured counterparts. Meanwhile, iGMSC-derived secretome contained a remarkable enrichment of both EVs and EV-free soluble peptide (SP) factors compared to that from 2D-GMSCs. The iGMSC-derived CM/secretome significantly enhanced skeletal muscle regeneration in a tongue defect model in rats. Our findings have provided valuable insight into the potential application of optimized GMSC-derived secretome products as cell-free therapeutics for regenerative therapy of tongue defects and other muscular diseases. However, the lack of standardized protocols for the preparation/characterization, formulation, and administration of MSC-derived secretome is one of the major obstacles to obtain the regulatory approval by The International Council for Harmonization of Technical Requirements for Pharmaceuticals for Human Use (ICH)[77]. Following the minimal criteria requirements for MSCs proposed by the International Society for Cellular Therapy (ISCT) [82] and the most recent Minimal Information for Studies of Extracellular Vesicle (MISEV) guidelines[83], our group has proposed to further optimize the protocols for production of iGMSC-derived secretome/EVs with consistent quality, stability, safety, and efficacy, which are important for the translation of the final product into clinical use.

Abbreviations

MSCs	Mesenchymal stem cells
GMSCs	Gingiva-derived mesenchymal stem cells
2D-GMSCs	Gingiva-derived mesenchymal stem cells cultured under standard 2D-monolay culture conditions
iGMSCs	Gingiva-derived mesenchymal stem cells cultured under defined xeno-free induction conditions
SIS	Small intestine submucosa
PLO	Poly-L-ornithine
CM	Conditioned culture media
EVs	Extracellular vesicles
SkMuSCs	Skeletal muscle stem cells
CHI3L1	Chitinase-3-like protein 1
STC1	Staniocalcin-1
IL-1RN	Interleukin 1 receptor antagonist
NAMPT	Nicotinamide phosphoribosyltransferase

Supplementary Information

The online version contains supplementary material available at https://doi.org/10.1186/s12951-025-03515-7.

Additional file 1.

Additional file 2 (Supplemental Figures).

Additional file 3 (Table S2).

Additional file 4 (Table S3).

Additional file 5 (Table S4).

Additional file 6 (Table S5).

Additional file 7 (Table S6).

Additional file 8 (Table S7).

Additional file 9 (Table S8).

Acknowledgements

Partial art images in the Graphic abstract and figure illustrations were from Smart-Servier Medical Art (https://smart.servier.com/).

Author contributions
Q. Z.: conceptualization, investigation, methodology, visualization, project administration, funding acquisition; writing—original draft, review, and editing. P.H.: investigation; methodology; writing—review and editing. Shihong Shi: investigation; methodology. Q.X.: Investigation; methodology; writing—review and editing. E.G.: writing—review and editing. B.W.: writing—review and editing. R. S: writing—review and editing. A.L.: Conceptualization; supervision; project administration; funding acquisition; resources; writing—review and editing. All authors reviewed the manuscript and approved the final version of the manuscript.

Funding
This work was supported by R21(NIH/NIDCR) (A. L.), the Schoenleber funding support (A.L. and Q. Z.), and Rabinowitz Research Award (Q. Z.)

Data availability
No datasets were generated or analysed during the current study.

Declarations

Ethics approval and consent to participate
The protocol of GMSC isolation from healthy donors was approved by Institutional Review Board (IRB) of University of Pennsylvania (IRB# 816238). All animal procedures were approved by the Institutional Animal Care and Use Committee (IACUC) of University of Pennsylvania (IACUC#805451).

Consent for publication
All authors have approved the manuscript and agree for publication.

Competing interests
The authors declare no competing interests.

Author details
[1]Department of Oral & Maxillofacial Surgery & Pharmacology, School of Dental Medicine, University of Pennsylvania, 240 South 40Th Street, Philadelphia PA19004, USA. [2]Department of Oral & Maxillofacial Surgery, Penn Medicine Hospital of the University of Pennsylvania, Philadelphia PA19004, USA. [3]Department of Bioengineering, School of Engineering and Applied Science, University of Pennsylvania, Philadelphia PA19004, USA. [4]Department of Oral and Maxillofacial Surgery, Rutgers School of Dental Medicine, Newark NJ07103, USA.

Received: 25 October 2024 Accepted: 28 May 2025
Published online: 10 June 2025

References

1. Wang Y, Fang J, Liu B, Shao C, Shi Y. Reciprocal regulation of mesenchymal stem cells and immune responses. Cell Stem Cell. 2022;29:1515–30.
2. Uccelli A, Moretta L, Pistoia V. Mesenchymal stem cells in health and disease. Nat Rev Immunol. 2008;8:726–36.
3. Han Y, Yang J, Fang J, Zhou Y, Candi E, Wang J, Hua D, Shao C, Shi Y. The secretion profile of mesenchymal stem cells and potential applications in treating human diseases. Signal Transduct Target Ther. 2022;7:92.
4. Li C, Sun Y, Xu W, Chang F, Wang Y, Ding J. Mesenchymal stem cells-involved strategies for rheumatoid arthritis therapy. Adv Sci Weinh. 2024. https://doi.org/10.1002/advs.202305116.
5. Poblano-Pérez LI, Castro-Manrreza ME, González-Alva P, Fajardo-Orduña GR, Montesinos JJ. Mesenchymal stromal cells derived from dental tissues: immunomodulatory properties and clinical potential. Int J Mol Sci. 2024. https://doi.org/10.3390/ijms25041986.
6. Zaripova LN, Midgley A, Christmas SE, Beresford MW, Pain C, Baildam EM, Oldershaw RA. Mesenchymal stem cells in the pathogenesis and therapy of autoimmune and autoinflammatory diseases. Int J Mol Sci. 2023;24:16040.
7. Fernández-Garza LE, Barrera-Barrera SA, Barrera-Saldaña HA. Mesenchymal stem cell therapies approved by regulatory agencies around the world. Pharmaceuticals (Basel). 2023;16:1334.
8. Hoang DM, Pham PT, Bach TQ, Ngo ATL, Nguyen QT, Phan TTK, Nguyen GH, Le PTT, Hoang VT, Forsyth NR, et al. Stem cell-based therapy for human diseases. Signal Transduct Target Ther. 2022;7:272.
9. Cuadra B, Silva V, Huang YL, Diaz Y, Rivas C, Molina C, Simon V, Bono MR, Morales B, Rosemblatt M, et al. The immunoregulatory and regenerative potential of activated human stem cell secretome mitigates acute-on-chronic liver failure in a rat model. Int J Mol Sci. 2024. https://doi.org/10.3390/ijms25042073.
10. Smolinská V, Boháč M, Danišovič Ľ. Current status of the applications of conditioned media derived from mesenchymal stem cells for regenerative medicine. Physiol Res. 2023;72:S233-s245.
11. Takahashi J. Next steps in regenerative medicine. Cell Stem Cell. 2023;30:509–11.
12. Giovannelli L, Bari E, Jommi C, Tartara F, Armocida D, Garbossa D, Cofano F, Torre ML, Segale L. Mesenchymal stem cell secretome and extracellular vesicles for neurodegenerative diseases: Risk-benefit profile and next steps for the market access. Bioact Mater. 2023;29:16–35.
13. Lotfy A, AboQuella NM, Wang H. Mesenchymal stromal/stem cell (MSC)-derived exosomes in clinical trials. Stem Cell Res Ther. 2023;14:66.
14. Zhang K, Cheng K. Stem cell-derived exosome versus stem cell therapy. Nat Rev Bioeng. 2023. https://doi.org/10.1038/s44222-023-00064-2.
15. Giannasi C, Della Morte E, Cadelano F, Valenza A, Casati S, Dei Cas M, Niada S, Brini AT. Boosting the therapeutic potential of cell secretome against osteoarthritis: comparison of cytokine-based priming strategies. Biomed Pharmacother. 2024;170: 115970.
16. Tan F, Li X, Wang Z, Li J, Shahzad K, Zheng J. Clinical applications of stem cell-derived exosomes. Signal Transduct Target Ther. 2024;9:17.
17. Kim D, Lee AE, Xu Q, Zhang Q, Le AD. Gingiva-derived mesenchymal stem cells: potential application in tissue engineering and regenerative medicine - a comprehensive review. Front Immunol. 2021;12: 667221.
18. Zhang Q, Shi S, Liu Y, Uyanne J, Shi Y, Shi S, Le AD. Mesenchymal stem cells derived from human gingiva are capable of immunomodulatory functions and ameliorate inflammation-related tissue destruction in experimental colitis. J Immunol. 2009;183:7787–98.
19. Tolouei AE, Oruji F, Tehrani S, Rezaei S, Mozaffari A, Jahri M, Nasiri K. Gingival mesenchymal stem cell therapy, immune cells, and immunoinflammatory application. Mol Biol Rep. 2023;50:10461–9.
20. Xu Q, Shanti RM, Zhang Q, Cannady SB, O'Malley BW Jr, Le AD. A gingiva-derived mesenchymal stem cell-laden porcine small intestinal submucosa extracellular matrix construct promotes myomucosal regeneration of the tongue. Tissue Eng Part A. 2017;23:301–12.
21. Zhang Y, Shi S, Xu Q, Zhang Q, Shanti RM, Le AD. SIS-ECM laden with GMSC-derived exosomes promote taste bud regeneration. J Dent Res. 2019;98:225–33.
22. Zhang Q, Nguyen PD, Shi S, Burrell JC, Xu Q, Cullen KD, Le AD. Neural crest stem-like cells non-genetically induced from human gingiva-derived mesenchymal stem cells promote facial nerve regeneration in rats. Mol Neurobiol. 2018;55:6965–83.
23. Zhang Q, Nguyen P, Burrell JC, Zeng J, Shi S, Shanti RM, Kulischak G, Cullen DK, Le AD. Harnessing 3D collagen hydrogel-directed conversion of human GMSCs into SCP-like cells to generate functionalized nerve conduits. NPJ Regen Med. 2021;6:59.
24. Schepici G, Gugliandolo A, Mazzon E. Serum-free cultures: could they be a future direction to improve neuronal differentiation of mesenchymal stromal cells? Int J Mol Sci. 2022. https://doi.org/10.3390/ijms23126391.
25. Nikolits I, Nebel S, Egger D, Kreß S, Kasper C. Towards physiologic culture approaches to improve standard cultivation of mesenchymal stem cells. Cells. 2021;10:886.
26. Tan F, Qian C, Tang K, Abd-Allah SM, Jing N. Inhibition of transforming growth factor β (TGF-β) signaling can substitute for Oct4 protein in reprogramming and maintain pluripotency. J Biol Chem. 2015;290:4500–11.
27. Ifkovits JL, Addis RC, Epstein JA, Gearhart JD. Inhibition of TGFβ signaling increases direct conversion of fibroblasts to induced cardiomyocytes. PLoS ONE. 2014;9: e89678.
28. Tao Y, Yang Y, Yang Z, Wang L, Wang SQ, Zhao Y. Robust small molecule-aided cardiac reprogramming systems selective to cardiac fibroblasts. IScience. 2023;26: 108466.
29. Winston TS, Suddhapas K, Wang C, Ramos R, Soman P, Ma Z. Serum-free manufacturing of mesenchymal stem cell tissue rings using human-induced pluripotent stem cells. Stem Cells Int. 2019;2019:5654324.

30. Shi A, Heinayati A, Bao D, Liu H, Ding X, Tong X, Wang L, Wang B, Qin H. Small molecule inhibitor of TGF-β signaling enables robust osteogenesis of autologous GMSCs to successfully repair minipig severe maxillofacial bone defects. Stem Cell Res Ther. 2019;10:172.
31. Subramanian A, Tamayo P, Mootha VK, Mukherjee S, Ebert BL, Gillette MA, Paulovich A, Pomeroy SL, Golub TR, Lander ES, Mesirov JP. Gene set enrichment analysis: a knowledge-based approach for interpreting genome-wide expression profiles. Proc Natl Acad Sci U S A. 2005;102:15545–50.
32. Sherman BT, Hao M, Qiu J, Jiao X, Baseler MW, Lane HC, Imamichi T, Chang W. DAVID: a web server for functional enrichment analysis and functional annotation of gene lists (2021 update). Nucleic Acids Res. 2022;50:W216-w221.
33. Dong L, Zieren RC, Horie K, Kim CJ, Mallick E, Jing Y, Feng M, Kuczler MD, Green J, Amend SR, et al. Comprehensive evaluation of methods for small extracellular vesicles separation from human plasma, urine and cell culture medium. J Extracell Vesicles. 2020;10: e12044.
34. Yang Y, Wu Y, Yang D, Neo SH, Kadir ND, Goh D, Tan JX, Denslin V, Lee EH, Yang Z. Secretive derived from hypoxia preconditioned mesenchymal stem cells promote cartilage regeneration and mitigate joint inflammation via extracellular vesicles. Bioact Mater. 2023;27:98–112.
35. Papait A, Ragni E, Cargnoni A, Vertua E, Romele P, Masserdotti A, Perucca Orfei C, Signoroni PB, Magatti M, Silini AR, et al. Comparison of EV-free fraction, EVs, and total secretome of amniotic mesenchymal stromal cells for their immunomodulatory potential: a translational perspective. Front Immunol. 2022;13: 960909.
36. Veerman RE, Teeuwen L, Czarnewski P, Güclüler Akpinar G, Sandberg A, Cao X, Pernemalm M, Orre LM, Gabrielsson S, Eldh M. Molecular evaluation of five different isolation methods for extracellular vesicles reveals different clinical applicability and subcellular origin. J Extracell Vesicles. 2021;10: e12128.
37. Bachurski D, Schuldner M, Nguyen PH, Malz A, Reiners KS, Grenzi PC, Babatz F, Schauss AC, Hansen HP, Hallek M, Pogge von Strandmann E. Extracellular vesicle measurements with nanoparticle tracking analysis - an accuracy and repeatability comparison between NanoSight NS300 and ZetaView. J Extracell Vesicles. 2019;8:1596016.
38. Rajkowska G, Miguel-Hidalgo JJ. Glial pathology in major depressive disorder: an approach to investigate the coverage of blood vessels by astrocyte endfeet in human postmortem brain. Methods Mol Biol. 2019;1938:247–54.
39. Liu Q, Chen X, Liu C, Pan L, Kang X, Li Y, Du C, Dong S, Xiang AP, Xu Y, Zhang Q. Mesenchymal stem cells alleviate experimental immune-mediated liver injury via chitinase 3-like protein 1-mediated T cell suppression. Cell Death Dis. 2021;12:240.
40. Bartosh TJ, Ylostalo JH. Efficacy of 3D culture priming is maintained in human mesenchymal stem cells after extensive expansion of the cells. Cells. 2019. https://doi.org/10.3390/cells8091031.
41. Xia TT, Hu R, Shao CJ, Feng Y, Yang XL, Xie YP, Shi JX, Li JS, Li XM. Stanniocalcin-1 secreted by human umbilical mesenchymal stem cells regulates interleukin-10 expression via the PI3K/AKT/mTOR pathway in alveolar macrophages. Cytokine. 2023;162: 156114.
42. Bustos ML, Huleihel L, Meyer EM, Donnenberg AD, Donnenberg VS, Sciurba JD, Mroz L, McVerry BJ, Ellis BM, Kaminski N, Rojas M. Activation of human mesenchymal stem cells impacts their therapeutic abilities in lung injury by increasing interleukin (IL)-10 and IL-1RN levels. Stem Cells Transl Med. 2013;2:884–95.
43. Ouyang Y, Hong Y, Mai C, Yang H, Wu Z, Gao X, Zeng W, Deng X, Liu B, Zhang Y, et al. Transcriptome analysis reveals therapeutic potential of NAMPT in protecting against abdominal aortic aneurysm in human and mouse. Bioact Mater. 2024;34:17–36.
44. Wu G, Su Q, Li J, Xue C, Zhu J, Cai Q, Huang J, Ji S, Cheng B, Ge H. NAMPT encapsulated by extracellular vesicles from young adipose-derived mesenchymal stem cells treated tendinopathy in a "One-Stone-Two-Birds" manner. J Nanobiotechnology. 2023;21:7.
45. Műzes G, Sipos F. Mesenchymal stem cell-derived secretome: a potential therapeutic option for autoimmune and immune-mediated inflammatory diseases. Cells. 2022. https://doi.org/10.3390/cells11152300.
46. Yeh CJ, Sattler KM, Lepper C. Molecular regulation of satellite cells via intercellular signaling. Gene. 2023;858: 147172.
47. Wang X, Zhou L. The multifaceted role of macrophages in homeostatic and injured skeletal muscle. Front Immunol. 2023;14:1274816.
48. Goto A, Kokabu S, Dusadeemeelap C, Kawaue H, Matsubara T, Tominaga K, Addison WN. Tongue muscle for the analysis of head muscle regeneration dynamics. J Dent Res. 2022;101:962–71.
49. Long R, Wang S. Exosomes from preconditioned mesenchymal stem cells: tissue repair and regeneration. Regen Ther. 2024;25:355–66.
50. Soukup R, Gerner I, Mohr T, Gueltekin S, Grillari J, Jenner F. Mesenchymal stem cell conditioned medium modulates inflammation in tenocytes: complete conditioned medium has superior therapeutic efficacy than its extracellular vesicle fraction. Int J Mol Sci. 2023. https://doi.org/10.3390/ijms241310857.
51. Mitchell R, Mellows B, Sheard J, Antonioli M, Kretz O, Chambers D, Zeuner MT, Tomkins JE, Denecke B, Musante L, et al. Secretome of adipose-derived mesenchymal stem cells promotes skeletal muscle regeneration through synergistic action of extracellular vesicle cargo and soluble proteins. Stem Cell Res Ther. 2019;10:116.
52. Giannasi C, Niada S, Magagnotti C, Ragni E, Andolfo A, Brini AT. Comparison of two ASC-derived therapeutics in an in vitro OA model: secretome versus extracellular vesicles. Stem Cell Res Ther. 2020;11:1–15.
53. González-Cubero E, González-Fernández ML, Olivera ER, Villar-Suárez V. Extracellular vesicle and soluble fractions of adipose tissue-derived mesenchymal stem cells secretome induce inflammatory cytokines modulation in an in vitro model of discogenic pain. Spine J. 2022;22:1222–34.
54. Ragni E, Perucca Orfei C, de Girolamo L. Secreted factors and extracellular vesicles account for the immunomodulatory and tissue regenerative properties of bone-marrow-derived mesenchymal stromal cells for osteoarthritis. Cells. 2022. https://doi.org/10.3390/cells11213501.
55. Zohora FT, Aliyu M, Saboor-Yaraghi AA. Secretome-based acellular therapy of bone marrow-derived mesenchymal stem cells in degenerative and immunological disorders: a narrative review. Heliyon. 2023;9: e18120.
56. Pincela Lins PM, Pirlet E, Szymonik M, Bronckaers A, Nelissen I. Manufacture of extracellular vesicles derived from mesenchymal stromal cells. Trends Biotechnol. 2023;41:965–81.
57. Noor Azlan NAB, Vitus V, Nor Rashid N, Nordin F, Tye GJ, Zaman WK. Human mesenchymal stem cell secretomes: Factors affecting profiling and challenges in clinical application. Cell Tissue Res. 2024;395:227–50.
58. Li J, Wu Z, Zhao L, Liu Y, Su Y, Gong X, Liu F, Zhang L. The heterogeneity of mesenchymal stem cells: an important issue to be addressed in cell therapy. Stem Cell Res Ther. 2023;14:381.
59. Dunn CM, Kameishi S, Grainger DW, Okano T. Strategies to address mesenchymal stem/stromal cell heterogeneity in immunomodulatory profiles to improve cell-based therapies. Acta Biomater. 2021;133:114–25.
60. Su Y, Xu C, Cheng W, Zhao Y, Sui L, Zhao Y. Pretreated mesenchymal stem cells and their secretome: enhanced immunotherapeutic strategies. Int J Mol Sci. 2023. https://doi.org/10.3390/ijms24021277.
61. Isaac J, Nassif A, Asselin A, Taïhi I, Fohrer-Ting H, Klein C, Gogly B, Berdal A, Robert B, Fournier BP. Involvement of neural crest and paraxial mesoderm in oral mucosal development and healing. Biomaterials. 2018;172:41–53.
62. Boddupally K, Wang G, Chen Y, Kobielak A. Lgr5 marks neural crest derived multipotent oral stromal stem cells. Stem Cells. 2016;34:720–31.
63. Zhang Q, Burrell JC, Zeng J, Motiwala FI, Shi S, Cullen DK, Le AD. Implantation of a nerve protector embedded with human GMSC-derived Schwann-like cells accelerates regeneration of crush-injured rat sciatic nerves. Stem Cell Res Ther. 2022;13:263.
64. Galipeau J. Macrophages at the nexus of mesenchymal stromal cell potency: the emerging role of chemokine cooperativity. Stem Cells. 2021;39:1145–54.
65. Peshkova M, Korneev A, Suleimanov S, Vlasova II, Svistunov A, Kosheleva N, Timashev P. MSCs' conditioned media cytokine and growth factor profiles and their impact on macrophage polarization. Stem Cell Res Ther. 2023;14:142.
66. Leñero C, Kaplan LD, Best TM, Kouroupis D. CD146+ Endometrial-derived mesenchymal stem/stromal cell subpopulation possesses exosomal secretomes with strong immunomodulatory miRNA attributes. Cells. 2022. https://doi.org/10.3390/cells11244002.
67. Xu Z, Lin L, Fan Y, Huselstein C, De Isla N, He X, Chen Y, Li Y. Secretome of mesenchymal stem cells from consecutive hypoxic cultures promotes resolution of lung inflammation by reprogramming anti-inflammatory macrophages. Int J Mol Sci. 2022;23:4333.
68. Holthaus M, Santhakumar N, Wahlers T, Paunel-Görgülü A. The secretome of preconditioned mesenchymal stem cells drives polarization and

reprogramming of M2a macrophages toward an IL-10-producing phenotype. Int J Mol Sci. 2022. https://doi.org/10.3390/ijms23084104.
69. Xu N, Bo Q, Shao R, Liang J, Zhai Y, Yang S, Wang F, Sun X. Chitinase-3-Like-1 promotes M2 macrophage differentiation and induces choroidal neovascularization in neovascular age-related macular degeneration. Invest Ophthalmol Vis Sci. 2019;60:4596–605.
70. Oh JY, Ko JH, Lee HJ, Yu JM, Choi H, Kim MK, Wee WR, Prockop DJ. Mesenchymal stem/stromal cells inhibit the NLRP3 inflammasome by decreasing mitochondrial reactive oxygen species. Stem Cells. 2014;32:1553–63.
71. Harrell CR, Markovic BS, Fellabaum C, Arsenijevic N, Djonov V, Volarevic V. The role of Interleukin 1 receptor antagonist in mesenchymal stem cell-based tissue repair and regeneration. BioFactors. 2020;46:263–75.
72. Lee KC, Lin HC, Huang YH, Hung SC. Allo-transplantation of mesenchymal stem cells attenuates hepatic injury through IL1Ra dependent macrophage switch in a mouse model of liver disease. J Hepatol. 2015;63:1405–12.
73. Fukada SI, Uezumi A. Roles and heterogeneity of mesenchymal progenitors in muscle homeostasis, hypertrophy, and disease. Stem Cells. 2023;41:552–9.
74. Wang YH, Wang DR, Guo YC, Liu JY, Pan J. The application of bone marrow mesenchymal stem cells and biomaterials in skeletal muscle regeneration. Regen Ther. 2020;15:285–94.
75. Sandonà M, Esposito F, Cargnoni A, Silini A, Romele P, Parolini O, Saccone V. Amniotic membrane-derived stromal cells release extracellular vesicles that favor regeneration of dystrophic skeletal muscles. Int J Mol Sci. 2023;24:12457.
76. MacDonald AF, Gross AJ, Jones BJ, Dhar MS. Muscle regeneration of the tongue: a review of current clinical and regenerative research strategies. Tissue Eng Part B Rev. 2022;28:1022–34.
77. da Silva AV, Serrenho I, Araújo B, Carvalho AM, Baltazar G. Secretome as a tool to treat neurological conditions: are we ready? Int J Mol Sci. 2023. https://doi.org/10.3390/ijms242216544.
78. Hodgson-Garms M, Moore MJ, Martino MM, Kelly K, Frith JE. Proteomic profiling of iPSC and tissue-derived MSC secretomes reveal a global signature of inflammatory licensing. NPJ Regen Med. 2025;10:7.
79. Kang M, Jordan V, Blenkiron C, Chamley LW. Biodistribution of extracellular vesicles following administration into animals: a systematic review. J Extracell Vesicles. 2021;10: e12085.
80. Liu L, Liu W, Han Z, Shan Y, Xie Y, Wang J, Qi H, Xu Q. Extracellular vesicles-in-hydrogel (EViH) targeting pathophysiology for tissue repair. Bioact Mater. 2025;44:283–318.
81. Li X, Zhang D, Yu Y, Wang L, Zhao M. Umbilical cord-derived mesenchymal stem cell secretome promotes skin regeneration and rejuvenation: from mechanism to therapeutics. Cell Prolif. 2024;57: e13586.
82. Galipeau J, Krampera M, Barrett J, Dazzi F, Deans RJ, DeBruijn J, Dominici M, Fibbe WE, Gee AP, Gimble JM, et al. International society for cellular therapy perspective on immune functional assays for mesenchymal stromal cells as potency release criterion for advanced phase clinical trials. Cytotherapy. 2016;18:151–9.
83. Welsh JA, Goberdhan DCI, O'Driscoll L, Buzas EI, Blenkiron C, Bussolati B, Cai H, Di Vizio D, Driedonks TAP, Erdbrügger U, et al. Minimal information for studies of extracellular vesicles (MISEV2023): From basic to advanced approaches. J Extracell Vesicles. 2024;13: e12404.

Publisher's Note